The Abdus Salam
International Centre for Theoretical Physics

2332

School on Synchrotron and FEL Based Methods and their Multi-Disciplinary Applications

19 - 30 March 2012

Additional information lecture Dr. M. Kiskinova

M. Kiskinova
Sincrotone, Trieste

J. Phys.: Condens. Matter **22** (2010) 000000 (23pp) UNCORRECTED PROOF

TOPICAL REVIEW

Transmission and emission x-ray microscopy: operation modes, contrast mechanisms and applications

Q.1 **Burkhard Kaulich**[1,3], **Pierre Thibault**[2], **Alessandra Gianoncelli**[1] **and Maya Kiskinova**[1]

[1] ELETTRA—Sincrotrone Trieste, Strada Statale 14, km 163.5 in Area Science Park, I-34149 Trieste-Basovizza, Italy
[2] Physics Department (E17), Technical University Munich, James-Franck-Straße, D-85748 Garching, Germany

E-mail: burkhard.kaulich@elettra.trieste.it

(Ed: Janet Thomas)
Ascii/Word/JPCM/
cm220805/TOP
Printed 30/12/2010
Spelling US
Issue no
Total pages
First page
Last page
File name
Date req
Artnum
Cover date

Received 14 September 2010, in final form 2 December 2010, accepted for publication 16 December 2010
Published
Online at stacks.iop.org/JPhysCM/22/000000

Abstract
Advances in microscopy techniques based on x-rays have opened unprecedented opportunities in terms of spatial resolution, combined with chemical and morphology sensitivity, to analyze solid, soft and liquid matter. The advent of ultrabright third and fourth generation photon sources and continuous development of x-ray optics and detectors has pushed the limits of imaging and spectroscopic analysis to structures as small as a few tens of nanometers. Specific interactions of x-rays with matter provide elemental and chemical sensitivity that have made x-ray spectromicroscopy techniques a very attractive tool, complementary to other microscopies, for characterization in all actual research fields. The x-ray penetration power meets the demand to examine samples too thick for electron microscopes implementing 3D imaging and recently also 4D imaging which adds the time resolution as well. Implementation of a variety of phase contrast techniques enhances the structural sensitivity, especially for the hard x-ray regime. Implementation of lensless or diffraction imaging helps to enhance the lateral resolution of x-ray imaging to the wavelength dependent diffraction limit.

Q.2 (Some figures in this article are in colour only in the electronic version)

Contents

1. Introduction 2
1.1. General remarks and organization of the review 2
1.2. Historical comments 2
2. X-ray sources and x-ray optics 3
2.1. X-ray sources 3
2.2. X-ray optics 3
3. Real-space imaging and microscopy techniques 4
3.1. Projection x-ray microscopes 4
3.2. Full-field imaging or transmission x-ray microscopes 4
3.3. Scanning x-ray microscopes 5
4. Contrast mechanisms in real-space transmission and emission x-ray microscopes 6
4.1. Absorption contrast 7
4.2. Phase contrast approaches 7
4.3. Darkfield imaging 10
4.4. X-ray fluorescence contrast 10
5. Diffraction x-ray imaging 11
5.1. Diffraction microscopy 11
5.2. Fourier transform holography 13

[3] Author to whom any correspondence should be addressed.

 © 2010 IOP Publishing Ltd Printed in the UK & the USA

5.3. Curved wavefronts and ptychography 13
6. Modern x-ray microscopes and their applications 14
6.1. SXM at beamline ID21 of the European Synchrotron Radiation Facility 14
6.2. Laboratory soft x-ray TXM using a compact laser plasma source at BIOX, KTH Stockholm 14
6.3. XM-2 at the Advanced Light Source 15
6.4. High-resolution x-ray imaging methods at the Advanced Photon Source 15
6.5. NanoXAS at the Swiss Light Source 16
6.6. The TwinMic microscope at Elettra 16
6.7. Magnetic imaging at the Advanced Light Source 17
6.8. Nano-imaging and nano-analysis project NiNa at the European Synchrotron Facility 18
6.9. The Nanoscopium project at Soleil 18
6.10. The hard x-ray fluorescence microprobe beamline at the Australian source 18
7. Concluding remarks and perspectives 18
Acknowledgments 19
References 20

1. Introduction

1.1. General remarks and organization of the review

The first visible light microscopes date back to the late 16th century, and since then advances in microscopy using different wavelengths of light and particles, such as electrons, ions and neutrons, have opened new perspectives for life and material science. Microscopy using x-rays as an illumination source is among the latest developments thanks to the invention of highly brilliant light sources and the fabrication of optical elements that allow focusing of the x-rays to nm dimensions. X-ray microscopy techniques using shorter wavelengths than visible light and appropriate photon optics have a resolving power that fills the gap between visible light and electron microscopy. Electron microscopes have reached atomic resolution but due to the short penetration length of the electrons and the vacuum environment they impose severe limitations on the specimen thickness ($<$100 nm) and state (dry or frozen hydrated specimen slices). In comparison, x-ray microscopes can image not only thicker specimens in their natural environment (e.g. whole cells) but the unique interactions of x-rays with matter allow control of the specimen chemical and physical properties which other microscopy techniques might not be able to detect. X-ray microscopes have progressed rapidly in the last decades, and nowadays different types of x-ray microscopes find applications in almost all fields, from medicine and life sciences to geochemistry, environmental and earth research.

The classification of x-ray microscopy instruments is similar to that of other microscopes, and can be divided into the following three classes. The simplest is the projection microscope, where a small, highly divergent source projects an image with high magnification onto a spatially resolving detector. The second class includes imaging microscopes where incident light is condensed onto the specimen and an appropriate optical element generates a magnified image onto a spatially resolving detector. The third class includes scanning instruments, where the source is demagnified to a small spot and the specimen is raster-scanned across this microprobe, monitoring transmitted and/or emitted photons or charged particles.

In brief, x-ray microscopes are versatile and can be operated in different detector configurations, transmission and/or secondary emission modes, which determines their application fields (Kirz *et al* 1995, Howells *et al* 2006). In this topical review we focus on recent developments in the branch of photon-in and photon-out x-ray microscopes, responding to the increasing requests for them and the broadening of their applications.

The review is divided into several sections. After some historical remarks, section 2 provides a description of x-ray sources, x-ray optics and recent developments. Section 3 describes different approaches to real-space transmission and emission x-ray microscopes, with highlights of recent progress in instrumentation. Section 4 summarizes the imaging and contrast mechanisms used in real-space transmission and emission x-ray microscopes. Section 5 is dedicated to diffraction imaging as a complementary reciprocal space technique. Section 6 gives examples of modern microscopes and their applications. Section 7 concludes with an outlook and perspectives.

1.2. Historical comments

Kirz, one of the pioneers of x-ray microscopy, summarized in a whimsical look the history of x-ray microscopy as '*This is a story of spies, heroes, villains, false starts, and a brush with real fame.*' (Kirz and Jacobsen 2009).

The discovery of x-rays by Roentgen (1896) in 1895 led not only to a revolution in medical imaging but also in many other fields of modern science. Roentgen could have been only partially aware of the absorption and phase properties of x-rays, especially about the value of the complex refractive index preventing him from focusing his new light 'invention'. It was Einstein who first suggested that the refractive index of x-rays, being a bit smaller than unity, should be considered as well (Einstein 1918). This motivated Kirkpatrick and Baez to explore reflective grazing incidence optics inventing the crossed two-lens focusing system known today as Kirkpatrick–Baez (KB) mirrors (Kirkpatrick and Baez 1948).

A major key ingredient in the progress of x-ray microscopy in the last two decades is the development of tunable and bright synchrotron radiation sources, though recently high-resolution x-ray microscopes using laboratory x-ray sources with limited energy tunability have become available as well (Hertz *et al* 2003, Feser *et al* 2004, Hertz *et al* 2009).

The first synchrotron-based x-ray microscope was developed by Horowitz and Howell (1972). It was followed by Günter Schmahl and his group who built and operated the first synchrotron-based full-field imaging or transmission x-ray microscope (TXM) at the Deutsche Elektronenspeicherring for Synchrotron Radiation (DESY), Germany and at the ACO storage ring, France (Niemann *et al* 1974, 1976),

using holographically fabricated diffractive optics (Schmahl and Rudolph 1969). Independently, Kirz and his group developed the first scanning x-ray microscope (SXM) at the Stanford Synchrotron Radiation Light source (SSRL) and the National Synchrotron Light Source NSLS (Kenney *et al* 1984). The advent of low-emittance third generation synchrotron sources fostered x-ray microscopy developments with the first undulator microscopy beamline at the NSLS (Rarback *et al* 1990a), followed by a manifold of other microscopy stations worldwide.

Q.3

2. X-ray sources and x-ray optics

This section gives an overview of the background material necessary to understand the topics tackled in this review. It includes a short description of the different types of x-ray sources and gives a short description of Fresnel zone plates, the most commonly used photon optics in x-ray microscopy. A thorough description of all types of focusing optics (Michette 1986) and x-ray interactions with matter can be found in several previous reviews (Kirz *et al* 1995, Attwood 2004, Howells *et al* 2006). However, since all the contrast mechanisms used in x-ray microscopes are based on the interactions of the x-rays with the specimen, a short overview of these interactions is given in section 4. For the present review we classify the x-ray sources according to the following scheme: soft x-rays with photon energy, E_{ph}, <2 keV, intermediate x-ray range with E_{ph} from 2 to 4 keV and hard x-rays with $E_{ph} > 4$ keV.

2.1. X-ray sources

Types of x-ray sources range from conventional x-ray tubes and compact laboratory sources to the third generation x-ray synchrotron light sources and the emerging fourth generation free electron lasers. The main characteristics that distinguish these different sources are: source size, divergence, energy range, tunability, time structure, polarization and coherence. One of the most important characteristics of the x-ray sources is the brightness, measured as the photon flux per second, solid angle, photon energy bandwidth and source size.

Conventional x-ray tubes come in different designs (Hittorf, Coolidge, Siegbahn–Gelius type, among others). They can reach a maximum brightness of 3×10^8 ph/(s mrad DE/E mm^2) and have typical beam sizes of 1 mm in unfocused e-beam form or down to 10 μm in focused e-beam form with characteristic lines broader than 0.5 eV in non-monochromatized form (Gelius *et al* 1990). Conventional x-ray sources, attractive due to their compactness, are used in laboratory x-ray microscopes. However, due to the discrete nature of the emission lines, they lack energy tunability, which prevents some important spectroscopy applications such as x-ray absorption spectroscopy (XAS). Other laboratory sources are compact x-ray laser plasmas, which nowadays reach nm wavelengths and are successfully used in microscopes that can work in the water window (Hertz *et al* 2009). The water window defines x-rays in the energy range between the K-absorption edges of carbon and oxygen, where water is transparent and carbon containing matter is strongly absorbing. A notable approach is the application of a recently developed compact light source, which produces x-rays by having an electron beam meet a counter propagating laser beam, through a mechanism called inverse Compton scattering. The small size of the intersection point gives a highly coherent cone beam with a few milliradian angular divergences and a few per cent energy spreads (Pfeiffer *et al* 2007, Bech *et al* 2008).

In spite of the ongoing development of laboratory sources, synchrotron facilities remain nowadays the best x-ray sources available for imaging and spectromicroscopy (Attwood 2004). Synchrotron radiation is produced by deflecting the trajectory of an electron or positron beam traveling at relativistic speeds. The radiation is generated by bending the electron beam using electromagnets or more complex systems called insertion devices (undulators or wigglers). These devices, installed in the straight sections of the storage ring, force the electrons to make many wiggles instead of a single bend, which results in multiplication of the emitted x-ray intensity. Along with the high brightness, the tunable in energy synchrotron radiation is also partially coherent and polarized. The time structure goes down to the picosecond range, thus enabling a variety of time-resolved experiments as well.

Emerging free electron laser (FEL) facilities provide ultrafast (femtosecond range) and extremely intense ($>10^{12}$ photons per pulse) laser-like x-ray pulses, produced by a process of self-amplification of a spontaneous emission, which occurs when the accelerated electron pulse travels through the periodic magnetic structure of a very long undulator (Brau 1990). A key characteristic of FEL x-rays is that they are fully coherent, which opens the great opportunity to explore lensless imaging, namely coherent diffraction imaging, x-ray holography imaging, curved wavefront phase retrieval and ptychography (see section 5). Since the resolution of the lensless imaging is in principle only dependent on the x-ray wavelength, these techniques could overcome the limits in resolution imposed by the focusing optics used in 'traditional' x-ray microscopes.

2.2. X-ray optics

Almost all x-ray optics have counterparts in the commonly used visible light optics, such as zone plates, multilayer or refractive lenses, and can be classified according to their working principles as (i) diffractive optics, (ii) reflective optics, and (iii) refractive optics. The interest in imaging with reflective optics has grown rapidly in recent years, triggered by demonstrations such as sub-100 nm lateral resolution with hard x-rays using Kirkpatrick–Baez mirrors (Hignette *et al* 2007, Mimura *et al* 2010). Refractive lenses in a multi-array arrangement have allowed sub-micrometer demagnification of the x-ray source with sufficient transmission (Lengeler *et al* 1999, Schroer *et al* 2008, Schropp *et al* 2010). Capillary or multi-capillary optics are still limited to the μm-range and are commonly used for illuminating specimens or increasing the solid angular acceptance of emitted secondary x-rays but rarely for microprobe formation, except for lower-resolution projection imaging (Kumakhov 1990, 2000). However, the

majority of the operating soft x-ray microscopes uses zone plate diffractive optics, ZPs, suggested first by Rayleigh (1888) and Soret (1875). They are commonly fabricated by means of electron lithography (Sayre 1972, Kern *et al* 1984, Tennant *et al* 1990, David *et al* 1992) that nowadays can write sub-10 nm features providing ultimate diffraction efficiency or lateral resolution (Kang *et al* 2008, Chao *et al* 2007, Werner *et al* 2009, Vila-Comamala *et al* 2009).

Since in this review we focus on x-ray microscopes using ZP diffractive focusing optics we will briefly describe their characteristics and working principle. A more detailed description can be found, e.g., in Michette (1986) and Attwood (1999).

ZPs are circular diffraction gratings with a radially increasing line density. They were invented independently by Rayleigh (1888) and Soret (1875) and some historical papers are reprinted in Ojeda-Castaneda and Gomez-Reino (1996). Their focusing properties were first discussed in the 1950s by Myers and Baez (Myers 1951, Baez 1952). The first ZPs for x-rays were fabricated in the 1960s (Mollenstedt *et al* 1963) and later on Schmahl and Rudolph (1969) developed a method to fabricate ZPs with sub-100 nm lateral resolution by applying UV lithography. Nowadays, ZPs, mostly produced using e-beam lithography, have achieved excellent imaging performance in both the soft and hard x-ray regimes (Kern *et al* 1984, Spector *et al* 1997, Weiss *et al* 1998, Di Fabrizio *et al* 1999, Anderson *et al* 2000, Charalambous 2003, David *et al* 2003, Rehbein *et al* 2004, Chao *et al* 2005, Holmberg *et al* 2009).

ZP characteristics have been recently described in detail in Howells *et al* (2006). Here we wish only to emphasize the following three important ZP properties. The focal length of a ZP with radius r, an outermost smallest grating line width Δr in first order diffraction and linear approximation is defined by $f\lambda = 2r\Delta r$ where λ is the wavelength, i.e. ZPs are highly chromatic optics. The lateral resolution is proportional to the smallest outermost line width and is approximately given by $\delta \approx 1.22\Delta r$. The depth of focus is approximately $2\Delta r^2/\lambda$ and can become considerably small especially for soft x-rays and high lateral resolution optics.

ZPs achieve today sub-20 nm and approach the sub-10 nm lateral resolution (Chao *et al* 2009) and they can be extended to unconventional x-ray focusing devices (Di Fabrizio *et al* 2003a, Cojoc *et al* 2006, Sakdinawat and Liu 2008).

3. Real-space imaging and microscopy techniques

Real-space x-ray imaging and microscopy techniques can in general be classified into the following three types. Projection imaging can be considered as real-space lensless imaging, where a small diameter x-ray source projects the specimen onto a pixel-array detector. Scanning x-ray microscopies include all instruments where an x-ray microprobe is formed and the specimen is raster-scanned across it to acquire the image. Full-field transmission x-ray microscopes are instruments where the specimen is illuminated by a modestly focused x-ray source and an objective lens magnifies the image of the specimen onto a pixel-array detector.

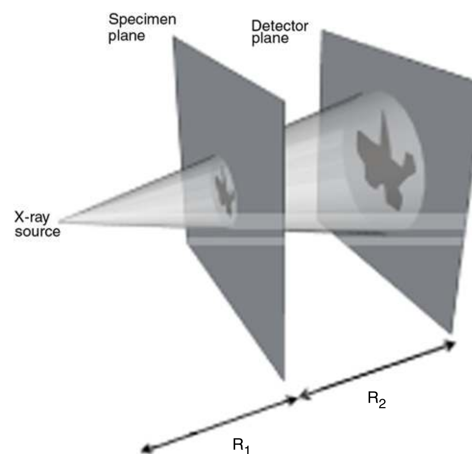

Figure 3.1. Scheme of a projection microscope with the source to specimen plane distance R_1 and specimen to detector distance R_2.

3.1. Projection x-ray microscopes

The principle of the projection x-ray technique (see figure 3.1) is to record a magnified shadow image by using a point source. This approach is similar to medical radiography, except that the medical instruments use a much larger x-ray source.

The magnification M of the projection x-ray microscope is given geometrically by the ratio of the distance R_1 of the x-ray source to the specimen and the distance R_2 from the specimen to the detector, $M = 1 + R_2/R_1$, and can easily be adjusted by varying the specimen position along the optical axis. The resolution Δ of the projection x-ray microscope is determined by the source size a. The image can be unsharpened due to Fresnel diffraction to $d = (\lambda z)^{1/2}$ where λ is the wavelength and z the propagation distance referred to the specimen plane (Nixon 1955). State-of-the-art theoretical optimization of lateral resolution has advanced far beyond the original work of Nixon *et al* and involves careful treatment of source size, detector resolution, wavelength and geometrical arrangement of optical components, especially if phase contrast imaging is approached (for example Pogani *et al* 1997). **Q.4**

Projection x-ray microscopes were invented in 1939 by Malsch and Ardenne (Germany) and the first instruments were developed by Cosslet and Nixon (Cosslet and Nixon 1951, Nixon 1955, Cosslet and Nixon 1960), and Newberry and Summers (1956). Yada and Takashaki used the focused electron beam of a scanning electron microscope as an x-ray source and achieved a resolution better than 0.2 μm at 1.7 keV photon energy (Yada and Takahashi 1992). A state-of-the-art instrument for projection microscopy, including phase-sensitive imaging and microtomography based on a converted scanning electron microscope, was reported for example by Mayo *et al* (2002), (2003a). Figure 3.2 shows a phase contrast data set and reconstructed cross section of a part of a ceramisphere acquired with the projection x-ray microscope of Wilkins' group at CSIRO, Australia (Mayo *et al* 2003a).

3.2. Full-field imaging or transmission x-ray microscopes

The full-field imaging x-ray microscope or transmission x-ray microscope (TXM) is an analogue of the visible light

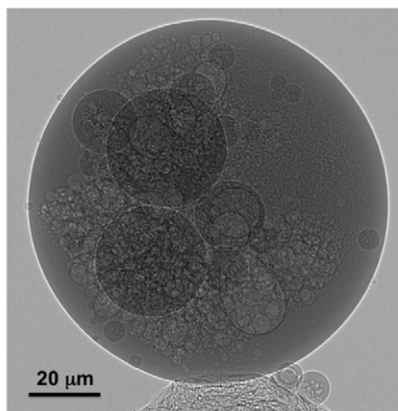

Figure 3.2. 3D phase contrast dataset view, reconstructed cross section of part of a ceramisphere, acquired with the projection x-ray microscope at the CSIRO, Australia. The total collection time of the microtomogram was 10 h. The diameter of the sphere is 110 μm (Mayo *et al* 2003a).

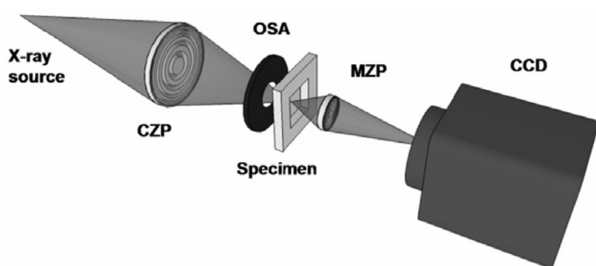

Figure 3.3. Optical scheme of a full-field imaging microscope (TXM) with x-ray source, condenser zone plate (CZP), specimen, the micro zone plate (MZP) functioning as objective lens, and charge-coupled device camera (CCD).

transmission microscopes and was pioneered by Schmahl, Rudolph and Niemann (Niemann *et al* 1976, Rudolph *et al* 1984). Usually a condenser optical element, typically condenser Fresnel zone plates (CZP), illuminates the specimen and an objective lens generates a magnified image of the specimen onto a two-dimensional detector (see figure 3.3). The approach of using ZPs both as condenser and objective lens is now well established and has been used by many groups, e.g. Meyer-Ilse *et al* (1995), Medenwaldt and Uggerhoj (1998), Le Gros *et al* (2005), Tsusaka *et al* (2001), Kagoshima *et al* (2003), Suzuki *et al* (2003), Takemoto *et al* (2003), Scott *et al* (2004), Youn *et al* (2005), Heim *et al* (2009), Pereiro *et al* (2009).

TXMs are static instruments that acquire a complete image on a direct imaging base. That is why they are best suited for morphological studies at the highest resolution, studies of dynamic events and microtomography.

In a TXM, all elements of the object field are illuminated and imaged simultaneously by a pixel detector. Independent imaging of each element of the object field is achieved when the object illumination is incoherent or partially coherent and the number of phase-space modes is equal to or larger than the number of detector pixels. Thus, the best imaging performance is obtained when the object is illuminated with a wide angle

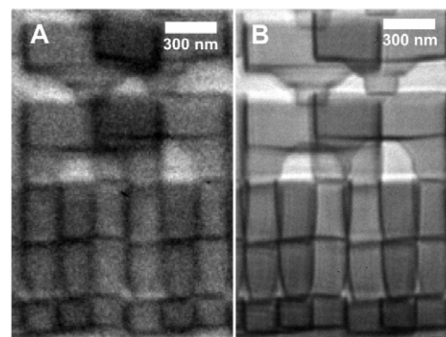

Figure 3.4. X-ray micrographs of a Cu/low-*k* on-chip interconnect stack, with the BESSY II TXM measured with a photon energy of 900 eV. Image A was obtained in first order of diffraction, energy resolution 4300, 5.2 s exposure time. Image B was obtained in third order of diffraction, energy resolution 1400, 26 s exposure time. The cut-off frequency in the power spectrum of image B corresponds to 12 nm feature size (Heim *et al* 2009).

and the numerical aperture is adapted to the objective lens (Jochum and Meyer-Ilse 1995). Consequently, bending magnet or laboratory sources are better suited than undulator sources, which have a much smaller phase-space area. However, since the undulator provides much higher flux, different approaches have been attempted to adapt the condenser system to such low-emittance sources (Niemann *et al* 2001, David *et al* 2003, Vogt *et al* 2006).

TXM excels at imaging samples with high lateral resolution and speed (see figure 3.4 for an example). On the other hand, its rigid configuration is not appropriate for parallel collection of complementary information using a multimodal approach. Combination with x-ray absorption spectroscopy is nevertheless possible by collecting a stack of images taken at different energies across a selected atomic absorption edge (Jacobsen *et al* 2000).

3.3. Scanning x-ray microscopes

Scanning x-ray microscopes (SXM) are a general class that includes scanning transmission x-ray microscopes (STXM) and different scanning photoemission microscopes, based on collection of emitted fluorescence x-rays or electrons.

SXM were pioneered in transmission mode (STXM) by the group of Janos Kirz (Kirz and Sayre 1980, Rarback *et al* 1990b). In a typical SXM apparatus, a virtual or secondary source is demagnified by a zone plate to form a microprobe across which the specimen is raster-scanned (see figure 3.5). Since the ZP has an infinite number of diffraction orders, a so-called order-selecting aperture (OSA) is placed between the ZP and the specimen in order to cut all undesired diffraction orders. The direct zero-order light through the ZP and OSA is blocked by a central stop (opaque area) on the ZP. The influence of the central stop on the image formation is described in Jochum and Meyer-Ilse (1995).

Unlike TXM, SXM requires a coherent illumination, in laser terms a single-mode illumination, to reach diffraction-limited lateral resolution. According to the van Cittert–Zernike theorem (Born and Wolf 1980), the degree of spatial coherence

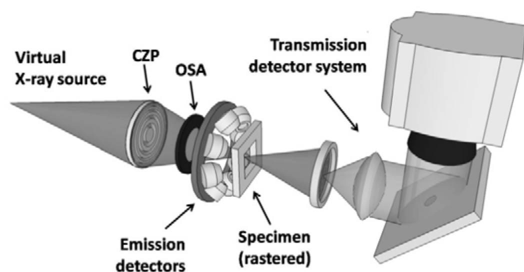

Figure 3.5. Optical scheme of the SXM imaging mode. A zone plate (ZP) in combination with an order-selecting aperture (OSA) forms a microprobe, across which the specimen is raster-scanned. Signals can be detected simultaneously by transmission and emission detectors.

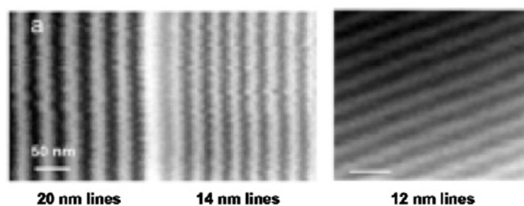

Figure 3.6. Resolution tests of the STXM at the ALS beamline 11.0.2 using a 20 nm outermost zone width ZP (Chao *et al* 2010). Left: absorption contrast x-ray micrographs of MoSi multilayer sections with indicated width. Middle: line profile on the 12 nm spaced multilayer with a maximum contrast of 7% at 800 eV photon energy. Right: absorption contrast x-ray micrographs of 80 nm thick Au structures with a vertical period of 40 nm. The absorption contrast is up to 65%. Figure courtesy of Tyliszczak.

is controlled by modifying the size of the effective source. Since the effective lateral resolution in SXM results from the convolution of the diffraction-limited point spread function, a good rule of thumb to maximize resolution while keeping a high flux is to set the geometrical demagnification of the source roughly equal to the diffraction-limited lateral resolution.

An example of state-of-the-art lateral resolution is given in figure 3.6, where Tyliszczak *et al* resolved with the environmental STXM instrument operated at the Advanced Light Source 12 nm line structures in MoSi multilayers with a maximum contrast of 7% (Chao *et al* 2010).

Due to the requirement of coherent illumination, SXM is typically operated at undulator sources and a wealth of instruments is available worldwide, e.g. Weitkamp *et al* (2000), Jacobsen *et al* (2002), Susini *et al* (2002), Kiskinova (2003), McNulty *et al* (2003), Suzuki *et al* (2003), Tyliszczak *et al* (2004), Menzel *et al* (2009). Instruments using bending magnets can also have excellent performance using appropriate spatial filtering of the source, e.g. Kilcoyne *et al* (2003), Suzuki *et al* (2003), Raabe *et al* (2008). Examples of state-of-the-art instruments and their applications are given in section 6.

Like other scanning probe techniques, SXM allows simultaneous monitoring of different signals, using appropriate x-ray or electron detectors. Thus simultaneous images of the transmitted x-rays and emitted fluorescence photons or electrons can be recorded. Scanning instruments are therefore well suited for a combination of imaging and spectroscopy, even at fixed incident photon energy, such as x-ray fluorescence spectroscopy and photoelectron spectroscopy. Another benefit of scanning microscopy is its flexibility in adjusting the field of view, which can be easily changed from large overview scans to high-resolution scans of selected small areas. The price to pay for this flexibility is an increased demand on the experimental setup, where the high positioning accuracy of the optical element typically requires the use of feedback systems.

As noted above, scanning instruments can work as x-ray fluorescence microscopes with appropriate dispersive x-ray detectors. μ-XRF spectrometers that make use of synchrotron radiation are described in section 6. The capabilities of scanning XRF microscopes using synchrotron radiation are not limited to elemental microanalysis but can be combined with transmission μ-XAS (Bohic *et al* 2005, Ade and Hitchcock 2008, Cotte *et al* 2010, Jacobsen *et al* 2003, Zhang *et al* 1994, Urquhart and Ade 2002) and 3D imaging (Rau *et al* 2001, Hitchcock *et al* 2008). In some instruments, simultaneous monitoring of absorption, phase contrast and darkfield imaging is implemented as well (Hornberger *et al* 2007, De Jonge *et al* 2008, Gianoncelli *et al* 2006, Stampanoni *et al* 2006). Micro x-ray diffraction (μ-XRD) (Maser *et al* 2006, Schroer *et al* 2010), scanning electron microscopes (Susini *et al* 2006) and scanning probe microscopes (Rodrigues *et al* 2008, Schmid *et al* 2010, Rose *et al* 2008) have also been implemented.

4. Contrast mechanisms in real-space transmission and emission x-ray microscopes

Contrast x-ray microscopes result from fundamental interactions of x-rays with matter. The primary processes are photon absorption (photoelectric effect), coherent (elastic or Thomson) scattering, and incoherent or inelastic (Compton) scattering.

X-ray absorption is mostly dominated by the interaction of x-rays with the core electrons of specimen constituent atoms. Atomic electron energy levels provide a means to obtain accurate elemental contrast through a resonant phenomenon, which results in well-defined discrete absorption edges. Already in 1946 Engström pointed out that the presence of a specific element can be obtained by acquiring images below and above its absorption edges (Engstrom 1946). Additional chemical information can be obtained by a careful measurement of detailed absorption fluctuations surrounding the selected atomic edge. X-ray absorption spectroscopy typically covers the immediate absorption edge region of a few 10 eV and can extend to energies hundreds of eV above the edge. Depending on the energy range the absorption spectroscopy is divided into two regimens: x-ray absorption near-edge spectroscopy (XANES) or near-edge x-ray absorption fine structure (NEXAFS), which provides information about the chemical state and bonding configuration of the absorbing atom, and extended x-ray absorption fine-structure spectroscopy (EXAFS), which is used to determine the coordination and bond distances to the neighboring atoms (Stohr 1992, Ade *et al* 1997).

Elastic scattering fundamentally takes place as dipole interactions with the material electron density. It is however tightly bound to absorption through the Kramers–Kronig

relation, which originates from causality conditions imposed on the impulse response function of the material (Als-Nielsen and McMorrow 2001). As long as x-ray polarization can be neglected, a scalar number conveniently expresses both absorption and elastic scattering, which is the complex-valued index of the material. As for all other ranges of the electromagnetic spectrum, the real part of the refraction index quantifies the propensity of matter to shift the incoming wave's phase, while the imaginary part is directly proportional to the total absorption cross section. Measurement methods based on the real part of the refractive index, grouped under the name of 'phase contrast imaging' make use of interference but are not necessarily interferometric (Gureyev 1999).

Absorption of an x-ray photon with sufficient energy ejects an electron, producing a short-lived core hole. In addition to the direct measurement of absorption amplitudes, x-ray emission spectroscopy relies on the physical phenomena that accompany absorption events. X-ray photoelectron spectroscopy (XPS) captures the primary ejected electrons and secondary electrons resulting from the de-excitation process (Siegbahn 1990). The first step of the de-excitation process is transition of an electron from a higher shell into the electron hole vacancy. The second step is a release of the energy difference, ΔE, via one of two processes: (i) emission of so-called Auger electrons with energy equal to or lower than ΔE and (ii) emission of photons with energy equal to ΔE, called fluorescence (Jenkins 1999). Auger emission dominates for photon energies below 1 keV, whereas the fluorescence photon emission dominates for higher photon energies and the ratio of fluorescence to Auger events is described by the fluorescence yield (Krause 1979). The fluorescent spectra of a given element are well defined by the energy states of the atom and the selection rules for allowed transitions, so the elemental content of a specimen can be determined by x-ray fluorescence microscopy. Since in the present review we exclusively discuss photon-in/photon-out microscopy techniques, further on we will give more detail and examples for application of x-ray fluorescence contrast.

4.1. Absorption contrast

Absorption imaging measures the attenuation of the x-ray beam as it travels through the specimen, very much like the x-ray radiographs commonly produced in hospitals. This imaging modality is by far the most widespread since it simply entails measuring directly the intensity of the x-rays transmitted through the specimen.

In an absorption micrograph, the lateral variations of contrast levels are determined by local density and attenuation cross sections of the constituent atoms for a given photon energy. Normally absorption images reveal the specimen morphology, but do not contain information about speciation corresponding to the different contrast levels. From a series of 2D images measured at different angles one can reconstruct through microtomography the 3D density of the specimen. Full information about the lateral elemental distribution and the local concentration of the elements and their chemical state can be obtained by taking images, tuning the photon energy below or above selected absorption edges of the constituent atoms. Such XANES images can provide a wealth of information, and statistical methods have also been used in their interpretation (Lerotic *et al* 2004). Full XANES spectra in different locations can be reconstructed from a stack of images or can be microprobed locally with the SXM setup by scanning the photon energy across the absorption edges. XANES spectra allow a fully quantitative analysis of the elemental and chemical distribution.

Q.5

4.2. Phase contrast approaches

Contrast techniques using the real, phase-shifting part of the complex refractive index are in many cases superior to absorption contrast for the following reasons: (i) the x-ray dose can be reduced dramatically, and (ii) the throughput is higher, because the phase shift dominates the absorption in the x-ray regime. Several phase-sensitive imaging approaches have been employed in the last decades. Among those are Bonse–Hart type interferometers (Bonse and Hart 1965, Momose *et al* 1995) or shearing interferometers (Kohmura *et al* 2003), grating interferometry (David *et al* 2002), and techniques including refraction measurements based on crystal diffraction (Pagot *et al* 2003). Propagation-based methods involve recovery of the object phase from one or more measurements of the object diffraction pattern such as in-line holography (Pagot *et al* 2003), holotomography (Cloetens *et al* 1999), iterative schemes (Allen *et al* 2001), wavefield propagation (Teague 1983, Paganin *et al* 2002), phase contrast projection microscopy (Mayo *et al* 2003b), or synchrotron-based non-interferometric techniques (Gureyev 1999). In this section, we will describe only the phase-sensitive imaging techniques applicable for real-space transmission x-ray microscopy.

4.2.1. Zernike phase contrast. Zernike phase contrast (Zernike 1935) is based on the segregation of non-deviated 'reference' and diffracted wavefronts emerging from the specimen, which are projected onto different locations in the objective rear focal or Fourier plane. The amplitude of the non-deviated wave is reduced in intensity and shifted in phase by $\pi/2$ (positive phase contrast) or $3\pi/2$ (negative phase contrast). The wavefront diffracted by the specimen is shifted in phase by $\pi/2$ and contrast is maximized because the reference and diffracted wave are fully in or out of phase.

Soft x-ray Zernike phase contrast was first demonstrated by Schmahl and Rudolph (1987, 1987, 1994, 1995) and optimized by Schneider (1998). Zernike phase contrast was recently extended to multi-keV radiation (Neuhausler *et al* 2003).

The relative phase retardation is a two-step process, as illustrated in figure 4.1. The condenser ZP annulus is constructed either as an opaque transparent annular ring in front of the condenser ZP or the zones of the condenser ZP are only structured within a small ring. The microscope condenser images the annular diaphragm to infinity, while the objective ZP images the diaphragm in its back-Fourier plane. In Koehler illumination, the back-Fourier plane of the objective ZP is conjugated to the front-Fourier plane of the condenser

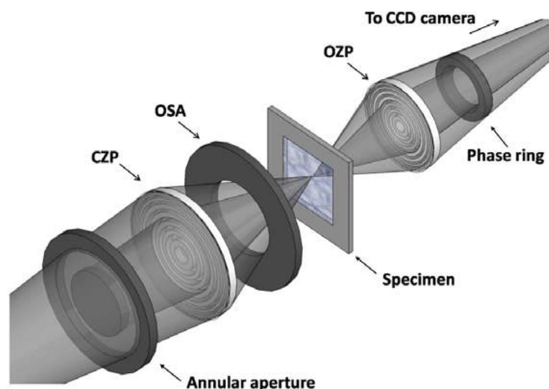

Figure 4.1. Schematic drawing of the optical microscope setup for Zernike phase contrast.

ZP, and the non-diffracted zero-order light forms an image of the condenser annulus in the back-Fourier plane of the objective lens. A phase ring mounted in or close to this plane selectively alters the phase and amplitude of the zero-order light. Figure 4.2 gives an example of Zernike phase contrast acquired with TXM at the ID21 beamline (Kaulich *et al* 1999, Susini *et al* 1999) of the European Synchrotron Radiation Facility (ESRF). The micrographs show microelectronic test structures with buried interconnects with notably stronger contrast in Zernike phase contrast compared to absorption imaging (Neuhausler *et al* 2003).

A major disadvantage of Zernike phase contrast is that artifact halos are introduced into the images due to the finite extension of the phase plate. This can be avoided by differential phase and interference contrast techniques as described in the following sections.

4.2.2. Differential phase contrast techniques. The image formation in STXM using a simple integrating detector, which collects the x-rays transmitted through the specimen, is equivalent to the incoherent absorption image in TXM. Scattering effects by the specimen lead to spatial variation of the signal and can give also phase contrast images using proper detectors. This is realized by the detector response function and segmenting the detector into arrays, which allows one to acquire anti-symmetrical signals and to recombine them by data processing, getting simultaneously absorption, differential phase contrast (DPC) and darkfield images. As the data processing is computationally not too demanding, the different contrast images can be visualized online during the raster scan with very little overhead time.

The theory of DPC in scanning mode with a split and first moment detector was pioneered in electron microscopy (Rose 1974, Hawkes 1978) and first explored with x-rays by Palmer and Morrison (1991). Chapman *et al* (1995) and Morrison *et al* (1987, 1996) were able to demonstrate DPC by collecting the entire two-dimensional pattern in the far-field for each pixel of the raster scan. The role of differential absorption contrast for DPC imaging has recently been described in Thibault *et al* (2009a, 2009b).

The first approach of DPC imaging uses a special configuration of integrating detectors, which can individually be read-out and recombined, summed-up or differentiated in order to provide different contrast such as absorption, differential phase contrast or darkfield images (Feser *et al* 2006, Hornberger *et al* 2008, De Jonge *et al* 2009).

The second approach is based on using a CCD camera as a configured detector (Morrison 1993, Gianoncelli *et al* 2006, Morrison *et al* 2006, Thibault *et al* 2009a, 2009b) with the advantage that the arrangement of the individual pixels or 'single detectors' is not pre-masked and masking is fully done computationally. This allows a wider versatility of data analysis, which becomes important when diffraction-type imaging such as ptychography (Rodenburg *et al* 2007a, 2007b, Thibault *et al* 2008) (see chapter 5) is combined with conventional real-space imaging. A major disadvantage of using a CCD camera compared to a segmented detector is its

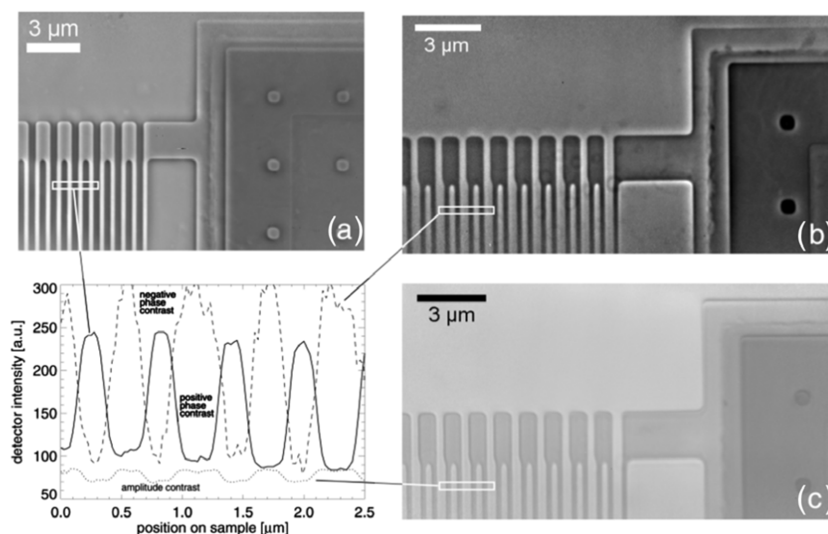

Figure 4.2. X-ray micrographs of a microelectronic test structure with the buried copper interconnect lines imaged in (a) positive phase contrast; (b) negative phase contrast and (c) absorption contrast mode. (d) The line scans across the serpentine structures demonstrate that Zernike phase contrast strongly enhances the image contrast and the visualization of weakly absorbing object details (Neuhausler *et al* 2003).

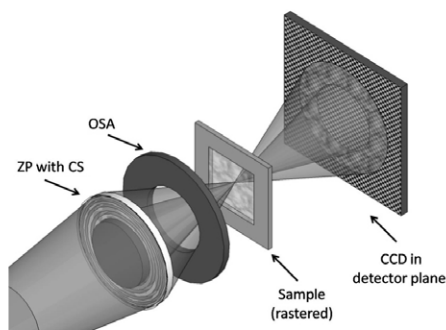

Figure 4.3. Configured detector in STXM mode. The integrating detector (photodiode) is replaced by a configured multi-element photodiode or CCD detector, which allows collection of the 2D pattern of the ZP diffraction cone modulated by the specimen in its far-field. Summing up all pixels gives the absorption contrast image, anti-symmetrical gravity-type analysis gives the differential phase contrast and collecting the signal in the segments outside the pattern the darkfield image.

Q.A

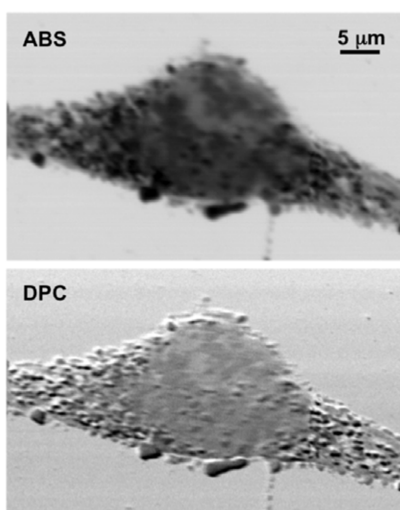

Figure 4.4. Absorption contrast (ABS) and DPC x-ray micrographs (DPC) simultaneously acquired with the TwinMic station (see chapter 6.5). The specimen provided by Ceccone and Marmorato from the EC Joint Research Joint Center in Ispra, Italy, is mouse 3T3 mouse fibroblast cells with incorporated $CoFe_2O_4$ nanoparticles. Photon energy: 705 eV.

typically slower read-out speed and the need for more time consuming online processing.

The potential of using a configured detector is demonstrated in figure 4.4, where a fast read-out electron-multiplier CCD camera with fast frame transfer and high sensitivity has been used to acquire simultaneously absorption and differential phase contrast images with the TwinMic x-ray microscope (see section 6.5). The specimen is a mouse 3T3 fibroblast cell with incorporated $CoFe_2O_4$ nanoparticles. Although the absorption image (ABS) shows good contrast, complementary information can be extracted from the edge enhancement in the DPC x-ray micrograph.

Another possible approach is a diffraction aperture-based differential phase contrast that can be implemented in STXM without adding any additional optical elements or configured

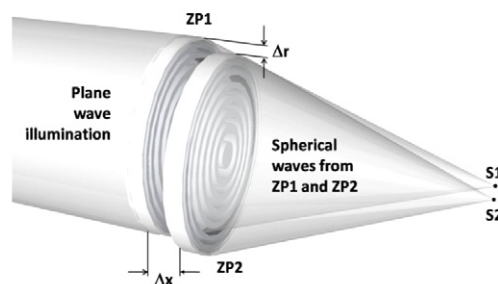

Figure 4.5. X-ray interference imaging with a ZP doublet. Beam splitting accomplished by ZP1 and ZP2 generates four waves in the image space. Apertures (not shown) block all combinations of other diffraction orders. Two spherical wave fronts originate from points S1 and S2 and interfere (Wilhein *et al* 2001).

detectors (Kaulich *et al* 2002a). An appropriate positioning and alignment of microscope apertures generates this DPC mode. Diffraction from the apertures produces a wave front with a non-uniform intensity distribution, which is imaged into the specimen area. The signal acquired with a pinhole photodiode located in the intensity gradient is highly sensitive to phase changes introduced by the specimen. This type of DPC approach is currently used at the SXM at the ID21 beamline of the ESRF (Susini *et al* 2002). The advantage of this setup is that it is very simple to align. The major drawback is its very low efficiency as only a very small portion of the signal is used.

A notable extension of DPC in combination with darkfield imaging (see chapter 3.2.6) is a multi-grating interferometer approach (David *et al* 2002), which has been successfully applied using laboratory sources (Pfeiffer *et al* 2009, Jensen *et al* 2010).

4.2.3. Differential interference contrast techniques. Nomarski-type differential interference contrast (DIC) for x-rays was first proposed by Polack and Joyeux using a Young's type slit setup in combination with a configured detector (Polack *et al* 1995, Joyeux *et al* 1999). Another optics-based approach has been successfully proven on the base of a ZP doublet setup (Wilhein *et al* 2001, Di Fabrizio *et al* 2002, Kaulich *et al* 2002b) similar to the one used a few decades ago for visible light interferometry (Murty 1963). The main advantages of this approach are that (i) this DIC technique leaves source and detector geometry invariant and can therefore be applied in STXM and in TXM mode, (ii) this approach is almost independent of the x-ray light coherence due to the small shear of the wave front division and small optical path differences, and (iii) it fits well to space constraints imposed by the very short ZP focal lengths using soft x-rays.

The interferometric principle for the STXM mode is illustrated in figure 4.5. In a very basic description, the two ZPs generate two spherical waves with laterally displaced foci by obstructing undesired ZP diffraction orders as far as possible.

Differential interference imaging means that the lateral focus separation is smaller than the lateral resolution. This means that interferometric imaging will not be affected by the degree of spatial coherence of the x-ray light, or the distance

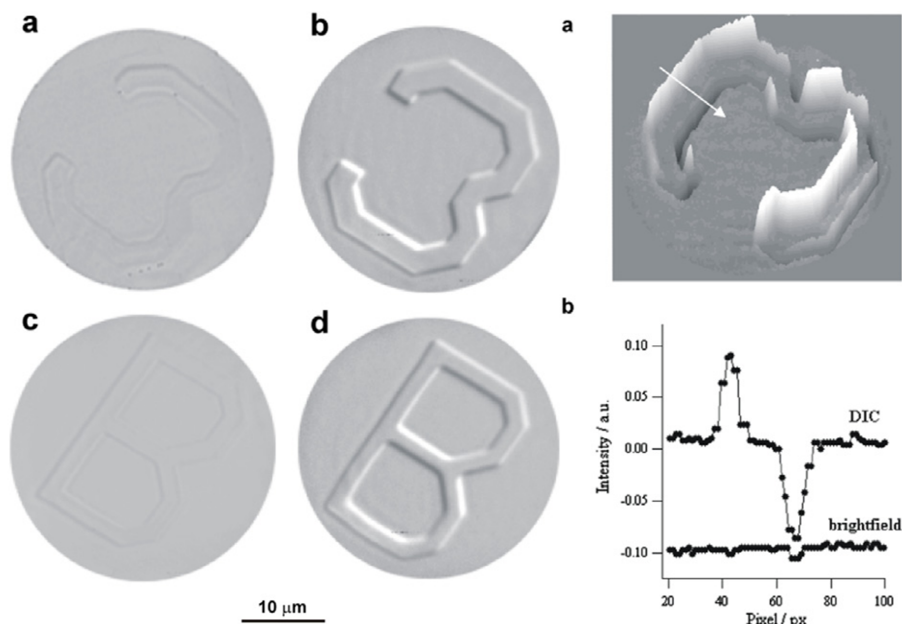

Figure 4.6. Comparison of absorption to DIC x-ray imaging. The structures show 2 μm thick PMMA test structures with 98.8% transmission at a photon energy of 4 keV; (a), (c) are absorption images and (b), (d) the corresponding DIC images. To demonstrate the increase in contrast, a line scan is plotted through the image of the same test structure. The images were acquired with the TXM at the ID21 beamline of the ESRF (Kaulich *et al* 2002b).

Δx of the Airy discs' maxima of both ZPs is smaller than their lateral resolution. Lateral displacement of the two optics has to be kept within the depth of focus of both ZP optics (Wilhein *et al* 2001).

Nomarski DIC techniques have been applied in both STXM and TXM instruments and figure 4.6 shows one of the first demonstrations, namely poly-methylmethacrylate (PMMA) structures imaged at 4 keV photon energy using the ESRF ID21 SXM (Barrett *et al* 1999). The 2 μm high structures have a transmission of 98.8% with a corresponding phase shift of $\phi = 0.706$ rad. Figure 4.6 documents the drastic increase in image contrast when DIC is applied.

Fabrication of such optics with lateral displacements within the lateral resolution of the optics (approximately smallest outermost ZP line width) and displacement along the optical axis requires tremendous effort in lithography techniques and also in integration of the two-ZP approach in a single unconventional ZP optics design (Di Fabrizio *et al* 2003b, Vogt *et al* 2005, Sakdinawat and Liu 2007).

4.3. Darkfield imaging

Darkfield or darkground imaging light is a mode where undiffracted zero-order is blocked in the optical scheme and only scattered light is detected. Darkfield microscopy is typically applied when the specimen consists of small scatterers with diffractive index close to the surrounding environment. The optical schemes for darkfield imaging in STXM and TXM are similar to the DPC setup and the Zernike phase contrast setup, respectively, with differences as illustrated in figure 4.7.

The first darkfield imaging with x-rays was reported by Morrison and Browne (1992), Suzuki and Uchida (1995) and

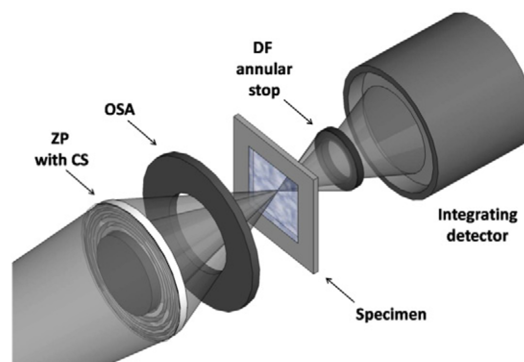

Figure 4.7. Schematic presentation of darkfield imaging in STXM mode. Either a darkfield stop is placed in front of the large-area integrating detector (photodiode) as shown here, or in the case of a configured detector only segments that do not intercept the direct unscattered light are considered for data analysis.

Chapman *et al* (1996) focusing on the importance of darkfield imaging for labeled cells. A comparison of darkfield in STXM and TXM modes is given in Vogt *et al* (2001). Darkfield imaging with laboratory sources is reported by Schwarzschild (2008), Pfeiffer *et al* (2009) and Jensen *et al* (2010) by using a grating interferometer approach. Figure 4.8 shows an example on forensics, where darkfield imaging helps to distinguish explosives from food products, such as, e.g., Swiss cheese, both having similar absorption cross sections but very different microstructure (Pfeiffer *et al* 2008).

4.4. X-ray fluorescence contrast

As described above, x-ray fluorescence (XRF) is the characteristic x-ray emission resulting from the de-excitation

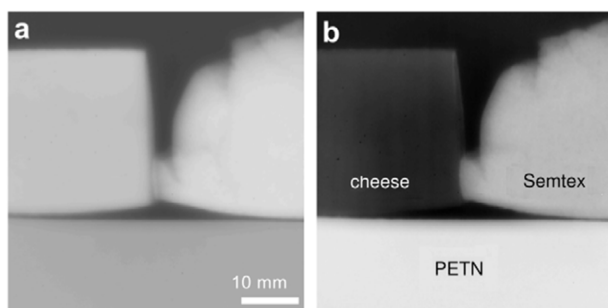

Figure 4.8. Conventional x-ray absorption (a) and darkfield image (b) of a cheese food product and the explosives 'PETN' and 'Semtex'. A differentiation of the explosives from the food product is impossible on the basis of the transmission image, but a distinct difference can be observed in the darkfield image. The granular microstructure, which is present in the explosives, causes strong small-angle scattering and the corresponding signal in the darkfield image (Pfeiffer *et al* 2009). Figure courtesy of Pfeiffer.

process after x-ray absorption and electron ejection, which is unique for each element. This makes XRF spectroscopy an excellent tool for elemental and chemical analysis. Many XRF spectrometers have been implemented in several instruments using laboratory x-ray sources (Stuik *et al* 1999), electron beams (EDX) (Reichelt 2006) or particle accelerators (PIXE) (Ortega *et al* 2009a). XRF covers a broad application range from extra-terrestrial (Sarrazin *et al* 2005) to sub-cellular research (Ide-Ektessabi 2007, Ortega *et al* 2009b), forensic science (Nishiwaki *et al* 2006) and cultural heritage (Cotte and Susini 2009). The increasing demand in science and technology to improve the spatial resolution for localization and speciation of trace elements in heterogeneous systems has been met by synchrotron XRF microscopes, where the high brightness and tunability of the x-ray source allow confining of the x-ray optical resolution down to sub-micrometer, preserving the high chemical sensitivity (Janssens *et al* 2000).

Q.8

Most of the modern scanning XRF microscopes operated in synchrotron facilities worldwide have configurations suited for detection of x-ray fluorescence emission in the keV range, involving the K, L and M electronic levels of medium- and high-Z elements (Salomé *et al* 2009, Kirkham *et al* 2010). The detection of light elements is hampered by the very low fluorescence yields. Anyhow, low-energy x-ray fluorescence (LEXRF) setups have recently been implemented in soft x-ray microscopes (Flank *et al* 2006, Alberti *et al* 2009) allowing detection of the lateral distribution of light elements with $Z > 3$, as will be shown in section 6.

The main advantage of combining XRF mapping with STXM microscopy is the possibility to collect simultaneously absorption and phase contrast images and the corresponding elemental distribution maps. Thus the specimen morphology can be directly correlated with the elemental distribution.

The possibility to combine the XRF setup with high brilliance micro- or nanobeam sources has also opened new opportunities in the field of XRF microtomography (Bleuet *et al* 2010), where several transmission and XRF image projections are collected by rotating and translating the specimen under the x-ray probe. This requires a high-precision goniometer and translation stages for the specimen and an appropriate algorithm to reconstruct the three-dimensional information.

5. Diffraction x-ray imaging

X-ray diffraction is among the most useful phenomena to probe matter at atomic scale. Crystalline materials, which produce sharp diffraction peaks, are especially well suited for in-depth investigation with high-energy x-rays. To date, the large majority of protein structures have been determined using x-ray crystallography. Even though x-ray scattering is very well understood and simply described using reciprocal space concepts, the problem of structure determination from x-ray diffraction data remains fundamentally difficult. The essence of these problems lies in the very measurement of diffracted radiation, in which only the amplitude is measured while the phase part of the diffracted wave is lost. The crystallographic 'phase problem' can be tackled nowadays with a multitude of efficient, though highly specialized methods.

In 1952, Sayre, inspired by a recent paper by Shannon (1949), suggested that the phase problem could be solved unambiguously if one had the ability to measure the scattered intensity between the Bragg diffraction peaks of a crystal (Sayre 1952). Interestingly, this statement does not concern the measurement process but rather dictates the required properties of the sample. Since a diffraction signal can be observed between Bragg peaks only if the crystalline symmetry is broken, the idea of applying Shannon's sampling concepts to diffraction makes it essentially a general imaging technique, in which no periodicity needs to be assumed. This early insight can be seen as the seed of modern diffractive imaging approaches (Sayre 1980).

Diffraction imaging also relates to Gabor's early work on holography (Gabor 1948), as it requires highly coherent sources. Transverse coherence ensures that the wave interacting with all parts of the sample is allowed to interfere completely with itself. The longitudinal coherence is required to avoid ambiguity in the scale of the momentum transfer or, in crystallographic terms, to avoid the superposition of multiple Ewald spheres in the signal. For x-rays, sufficient coherent flux came only with the second and especially third generation synchrotron sources, decades after Sayre and Gabor's initial proposals. By then, other x-ray microscopy methods were already being developed. Yet many have found that diffractive imaging efforts are worth pursuing. Among other motivations are the promises of reaching higher resolutions, thanks to the complete absence of lenses, which inevitably cause aberrations and signal losses.

A recent review on coherent methods in the x-ray sciences has been written by Nugent (2009).

5.1. *Diffraction microscopy*

In the classical form of diffractive imaging, often called diffraction microscopy, a sample is bathed in a planar, monochromatic and coherent wavefield, and the diffracted intensity is measured by a pixel-array detector in the far-field

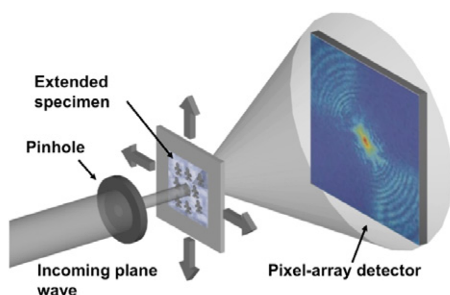

Figure 5.1. Schematic of a diffraction microscopy experimental setup. An incoming plane wave illuminates an isolated specimen. The diffraction pattern from the specimen is recorded on a pixel-array detector.

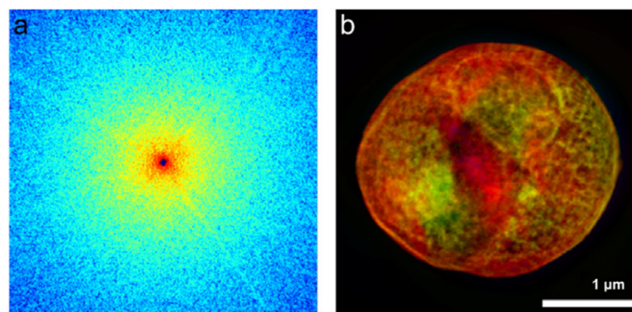

Figure 5.2. (a) Diffraction pattern of a yeast cell; (b) x-ray micrograph reconstructed from the diffraction pattern in (a). Figure adapted from Shapiro *et al* (2005).

(see figure 5.1). By a well-known property of Fraunhofer diffraction, the intensity measured in the detector plane is equal to the absolute value squared of the Fourier transform of the exit wave in the image plane. The coherence of the incident wave gives rise to a characteristic 'speckle pattern' in the diffraction plane. It is from this speckle pattern that real-space information on the specimen is extracted. As in crystallography, the phase problem is the main obstacle to the simple inversion of the diffraction pattern since given only the magnitudes of a Fourier transform, there exists an infinity of possible solutions to the problem, corresponding to all possible assignments of phases to the Fourier components.

For both technical and fundamental reasons, the diffraction pattern has to be sampled on a grid fine enough to satisfy Nyquist's criterion (Shannon 1949). According to Shannon's theorem, satisfying this so-called 'oversampling' condition ensures that the smooth diffraction pattern is known at all points within the detector area, provided that it is band-limited. In this context, 'band-limited' means that the sample has to occupy a sufficiently compact region of space (called the support), thus imposing the critical experimental constraint that the sample be isolated. The fact that most of the field of view is empty, as a result of the sample isolation, provides the required additional constraint to make the phase problem approachable.

Attempts at solving this type of problem—reconstructing a supported function from the amplitudes of its Fourier transform—seem to have been somewhat impeded by the early realization that the solution is never unique in one dimension (Wolf 1962, Walther 1963). An important step was made when Fienup obtained reproducible and apparently unique solutions of the two-dimensional problem using an iterative algorithm (Fienup 1978). It was then quickly realized that uniqueness is nearly guaranteed for problems in dimensions larger than one (Bruck and Sodin 1979, Bates 1982).

Fienup's early work, itself inspired by a method introduced by Gerchberg and Saxton (1972), has been influential in the field of diffractive imaging, especially in demonstrating the value of iterative algorithms to solve the phase problem. In recent years, Fienup's hybrid input–output algorithm (Fienup 1982) has inspired the development of other iterative methods, such as the difference map algorithm (Elser 2003a, 2003b), the shrink-wrap method (Marchesini *et al* 2003), and the relaxed averaged alternating reflections algorithm (Russel Luke 2005).

Initial x-ray speckle measurements were not suitable for reconstructions, either because of insufficient data quality (Yun *et al* 1987) or because of partial coherence and of the complexity of the specimen (Sutton *et al* 1991). The first complete demonstration of x-ray diffraction microscopy, the 'ABC' of diffraction microscopy, came about a decade later (Miao *et al* 1999). The last ten years saw a multiplication of demonstrations from various groups and facilities. Improvements of the original methodology have been gradually explored and mastered. The goals most actively pursued are the extension to three-dimensional imaging (Miao *et al* 2002, Chapman *et al* 2006a, Barty *et al* 2008, Barty 2008) and the application to biological specimens (Miao *et al* 2003, Shapiro *et al* 2005, Huang *et al* 2009, Lima *et al* 2009, Nishino *et al* 2009, Nelson *et al* 2010). Figure 5.2 demonstrates the performance of such approaches. Diffraction microscopy has been demonstrated with x-ray free electron laser sources (Chapman *et al* 2006b, Bogan *et al* 2008), high-harmonic generation sources (Sandberg *et al* 2008), and highly focused synchrotron hard x-rays (Schroer *et al* 2008). A surprising variant of the method consists in detecting the smooth diffuse diffraction surrounding the Bragg peak of a nanocrystal instead of the usual small-angle scattering signal (Williams *et al* 2003). This approach was shown to give access to selected components of the strain field within crystallites (Pfeifer *et al* 2006, Robinson and Harder 2009).

Because they do away with the optics, coherent diffractive imaging techniques are often seen as having the greatest potential for high-resolution. X-ray optics affect the image resolution in two distinct ways. First, the numerical aperture of a focusing device determines its achievable resolution (the diffraction limit). Second, zone plates and refractive lenses are made of partly absorptive materials that limit their efficiency to typically less than 25%, and often as low as a few per cent. While the former limitation evolves as improved focusing devices are fabricated, the latter is more fundamental. Image-forming optics waste a large fraction of the photons that interacted with the sample placed upstream. This problem is critical for high-resolution imaging of radiation-sensitive specimens because of the strong dose constraints (Shen *et al* 2004, Howells *et al* 2009). It is now known that radiation

limits can be overcome with the short and powerful pulses of x-ray free electron lasers by gathering a diffraction signal before damage is visible (Chapman *et al* 2006b). This fact, combined with the outstanding coherence properties of free electron sources, could help obtain 2D images with nanometer resolution on specimens such as biological cells (Bergh *et al* 2008). This 'diffract-and-destroy' approach could have especially far-reaching repercussions for specimens available in multiple identical copies, such as macromolecules and viruses, since it may permit 3D structure determination without resorting to crystallization (Neutze *et al* 2000).

Despite its promise and potential, diffraction microscopy remains technically challenging, especially because of the requirement that the sample be completely isolated. Attempts at imaging frozen hydrated biological cells in cryogenic conditions have up to now been mostly unsuccessful, in part because of the scattering from ice surrounding the sample (Sayre 2008). Besides sample isolation, diffraction microscopy is known for its relatively capricious phase retrieval process that suffers from small systematic imperfections in the data. Fourier transform holography, Fresnel diffraction imaging and ptychography are notable members of the coherent diffractive imaging family that overcome some of these limitations.

5.2. Fourier transform holography

Fourier transform holography, a technique nearly as old as holography itself (Gabor 1948, Stroke 1965), uses interference with an off-axis, punctual reference in the specimen plane. It is easily shown that the image of the object is obtained directly upon Fourier transformation of the measured diffraction pattern. In practice a point reference can be produced with a focusing device (McNulty *et al* 1992), but most recent realizations of the technique rather use small pinholes milled in absorbing membranes, with the sample of interest placed in a nearby window (Eisebitt *et al* 2004). The approach is compatible with single shot imaging (Barty *et al* 2008, Barty 2008, Ravasio *et al* 2009, Sandberg *et al* 2009), and can be used with a moving mask (Tieg *et al* 2010). In recent extensions of the method, allowable references include lines and corners (Guizar-Sicairos and Fienup 2007, Podorov *et al* 2007, Zhu *et al* 2010) as well as more complicated structures called 'uniform redundant arrays' (Marchesini *et al* 2008).

Fourier transform holography has clear benefits when compared to diffraction microscopy. First, an image is obtained immediately simply with a single fast Fourier transform (FFT) operation. Because it involves a linear transformation in intensity spaces, it remains valid with partially coherent illumination and even accommodates the incoherent sum of multiple diffraction patterns (Schlotter *et al* 2007). These benefits have a price. The sample preparation can be more complex and difficult, the oversampling requirement is stronger than for diffraction microscopy (by at least a factor of two) and the resulting image is degraded by the convolution with the reference illumination. The radiation dose is also higher than in diffraction microscopy for the same signal to noise ratio, since valuable information contained in the self-interference of the sample is not used in the data processing.

5.3. Curved wavefronts and ptychography

Fourier transform holography eliminates the reconstruction difficulties of diffraction microscopy through a physical encoding of the phase information. The other important limitation mentioned above, the requirement for an isolated sample, still remains to some extent. Making coherent diffractive imaging applicable to extended specimens requires that the oversampling condition be satisfied by other means. The most successful approach up to now is to limit the extent of the illumination instead of the sample itself. As simple as it may seem, moving away from planar wavefronts to finite, non-uniform illumination brings its own complications. First, phase retrieval is notoriously more difficult (and often impossible) as soon as the edges of the support are not sharp, as is typically the case with a propagated finite illumination. Second, even if phase retrieval somehow succeeds, the interpretation of the resulting exit wave may be very difficult because it is shaped both by the incoming wavefront and by the transmission function of the specimen.

One solution to these problems is to use a well-characterized curved illumination, as can be found away from the focal plane of focusing optics (Nugent *et al* 2005). The far-field pattern for this special case is formally equivalent to a magnified near-field diffraction pattern—that is, a magnified in-line hologram. It has been shown that this method, coined 'Fresnel CDI', or 'keyhole CDI' yields especially well to simple phase retrieval algorithms (Williams *et al* 2006, Abbey *et al* 2008).

Another method, called ptychography, approaches the problem differently: information necessary to reconstruct the sample's transmission function is obtained by measuring multiple far-field diffraction patterns while changing the position of the illumination relative to the sample. Hardly a new technique, ptychography has nevertheless become popular among CDI practitioners only very recently.

Ptychography was first developed as a means to solve the crystallographic phase problem in electron microscopy (Hegerl and Hoppe 1970). Suggested by Hoppe and Hegerl, the method essentially was to broaden the Bragg reflections of a crystalline sample with a focused electron beam, in order to measure the interference between neighboring Bragg peaks. Measuring the diffraction patterns as the illumination is scanned within the crystal unit cell leads to 'super-resolution' compared to traditional scanning transmission electron microscopy (STEM) (Nellist *et al* 1995). The technique was found to be applicable to non-crystalline specimens as well. A single-step reconstruction technique based on the Wigner distribution formalism was developed in the early 1990s (Bates and Rodenburg 1989, Rodenburg and Bates 1992) and the first application of ptychography to x-rays was reported in 1996 by Chapman (1996, 1997). The technique entered a new development stage when it was shown that reconstructions could be obtained with simple and robust iterative algorithms (Faulkner and Rodenburg 2004, Rodenburg and Faulkner 2004, Faulkner and Rodenburg 2005, Rodenburg *et al* 2007a, 2007b). A recent review of ptychography up to this point of development has been published by Rodenburg, one of its key players (Rodenburg 2008).

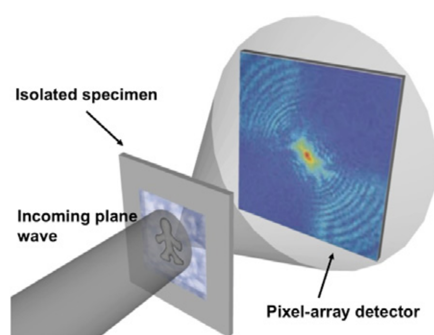

Figure 5.3. Schematic of a ptychography experimental setup. A compact coherent illumination is produced with a small pinhole (or a lens). Far-field diffraction patterns are measured for each position of the sample as it is scanned in the beam. The overlap of the illuminated areas of neighboring scan points creates redundancy in the data that is exploited to reconstruct the sample's image and the illumination profile.

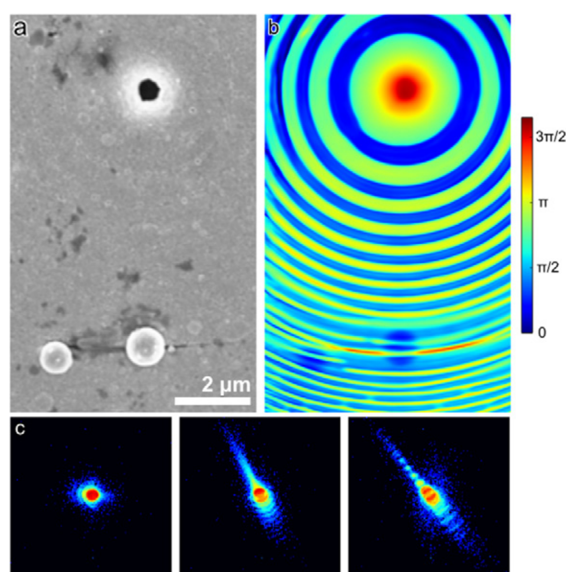

Q.B

Figure 5.4. Hard x-ray ptychography on a zone plate test specimen. (a) Scanning electron microscopy (SEM) image of a nanofabricated sample covered with gold. (b) Phase part of the transmission function obtained by ptychographic reconstruction. The color scale indicates the phase shift imposed by the sample on the incoming wave, and is proportional to the integrated thickness of the object. (c) Selection of individual diffraction patterns collected for this reconstruction. Figure adapted from Thibault *et al* (2008).

It is now known that ptychographic datasets can have such a high level of redundancy that no prior knowledge on the incoming illumination is required to reconstruct successfully the image of the sample (Guizar-Sicairos and Fienup 2008, Thibault *et al* 2008), as shown in figure 5.4. Now commonly used reconstruction algorithms extract both the sample's transmission function and the complex-valued illumination function from a single dataset. This new development has proven highly valuable to reduce reconstruction artifacts (Maiden and Rodenburg 2009, Thibault *et al* 2009a, 2009b) and to characterize the wavefront produced by x-ray optics upstream from the sample (Kewish *et al* 2010a, Schropp *et al* 2010). Recent demonstrations with hard x-rays have shown the high sensitivity of the technique with weakly scattering biological samples (Dierolf *et al* 2010a, Giewekemeyer *et al* 2010), and the quantitative quality of the reconstructions was highlighted with the recent tomographic reconstruction of a bone sample (Dierolf *et al* 2010b).

The main restrictions of ptychography are relatively obvious: being a scanning technique, the total acquisition time can be long, and resolution can be limited by mechanical instabilities. In particular, it will have little application for the upcoming x-ray free electron lasers, except perhaps in special cases like structure determination from 2D crystals (Kewish *et al* 2010b).

6. Modern x-ray microscopes and their applications

6.1. SXM at beamline ID21 of the European Synchrotron Radiation Facility

Recently, the ID21 SXM (Susini *et al* 2004) has contributed to the elucidation of ancient opaque glass manufacturing processes (figure 6.1(A)). X-ray fluorescence mapping enables the identification and localization of micrometric crystals (figure 6.2(B)), whereas the XANES spectra measured with a sub-micrometric probe, specifically in the vitreous matrix embedding the crystals (figure 6.1(C)) provide more detailed chemical information. Although the instrument can work also in transmission mode, in this particular study of a very thick specimen the XANES spectra were obtained by monitoring the emitted total fluorescence yield. Spectra acquired on ancient products (Egyptian, Roman, etc) are compared with reference spectra of synthetic opaque glasses, obtained by *in situ* crystallization, e.g. introduction of Sb_2O_4 (red in figure 6.1(C)), or by addition of synthetic calcium antimonate crystals (blue in figure 6.1(C)). Combined with high-resolution transmission electron microscopy analyses, these experiments provide new hypotheses about ancient glass manufacturing processes in the antiquity. In particular, it is proven that Egyptian glassmakers synthesized nanocrystals of calcium antimonates, that were later on introduced into glass to opacify it (Lahlil *et al* 2010a, 2010b).

6.2. Laboratory soft x-ray TXM using a compact laser plasma source at BIOX, KTH Stockholm

The development of compact laboratory TXM is motivated by the limited access to synchrotron-based x-ray microscopes and the high request for x-ray microscopes optimized for daily characterization of particular materials.

We describe a type of TXM instrument developed at the BIOX facility of the KTH Stockholm, Sweden (Takman *et al* 2007, Hertz *et al* 2009), which works in the water window dedicated exclusively to studies of biological samples. This compact table-top TXM uses a soft x-ray emitting plasma source generated with a pulsed high-power laser ($\lambda = 532$ nm, 3 ns, 100 Hz, 100 mJ) focused onto the laminar flow of a liquid (methanol) jet. The photon flux of this source is approximately 5×10^{13} ph/(s sr) at 3.37 nm and the monochromaticity is better than 500. A normal incidence Cr/Sc multilayer mirror monochromatizes and condenses the

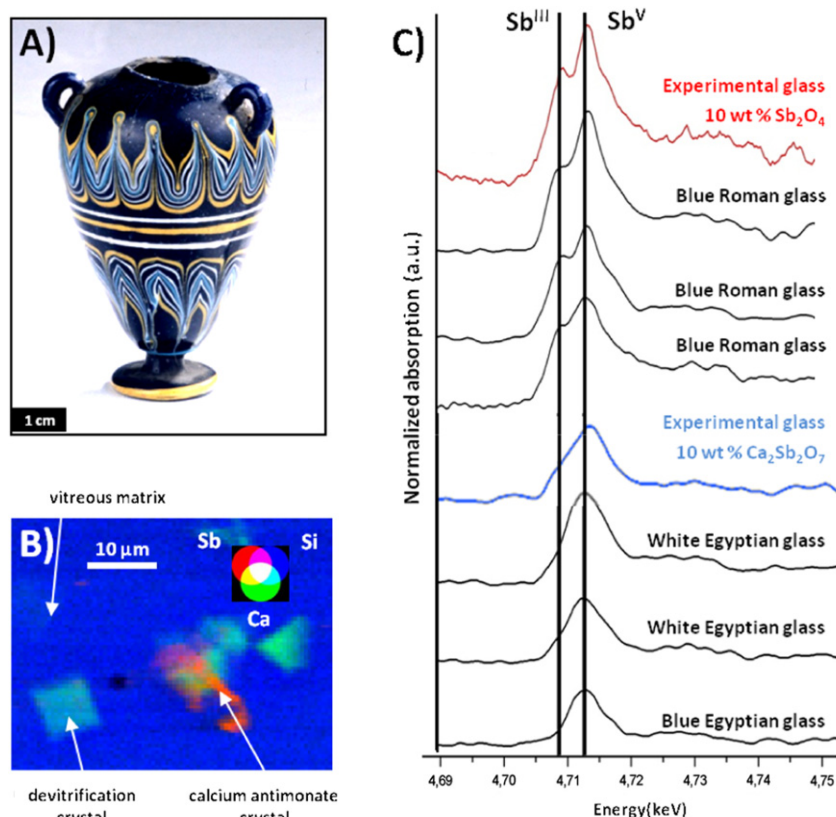

Figure 6.1. Determination of Sb oxidation state in ancient glasses, opacified by the presence of calcium antimonate crystals. (A) Opaque colored glass of the 18th Egyptian dynasty—small amphorae (inventory number AF2622; ©D Bagault C2RMF). (B) $46 \times 36\ \mu m^2$ XRF maps showing the Sb, Ca and Si elemental distribution, measured with $1.1 \times 0.3\ \mu m^2$ x-ray microprobe size. Micrometric devitrification crystals as well as calcium antimonate crystals are identified. (C) μ-XANES spectra of ancient glasses acquired at the Sb L_I-edge, and reference spectra (red and blue) of glasses synthesized in the laboratory. The Sb oxidation state in the glass matrix keeps the memory of the Sb oxidation state in the ingredients used for the glass synthesis. In particular, the Sb(III)/Sb(V) ratio is the characteristic value in the different products (Lahlil *et al* 2010a, 2010b).

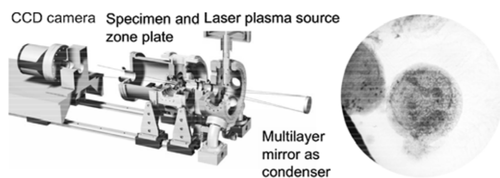

Figure 6.2. Left: scheme of a compact table-top TXM at the BIOX, KTH Stockholm facility, Sweden, with a laser plasma liquid jet source and a normal incidence multilayer mirror as condenser optical element; right: x-ray micrograph of a human immune C-cell (721.224/HLA-Cw6). The cell is about 15 μm in diameter. Figure courtesy of Ulrich Vogt.

x-ray light into the specimen plane with an average flux of 2×10^6 ph s^{-1}. The specimen is magnified by in-house fabricated zone plates (Holmberg *et al* 2009) onto a CCD detector (see figure 6.2). The instrument can operate in phase contrast imaging (Bertilson *et al* 2008) and tomography (Bertilson *et al* 2008) modes, and can reach lateral resolutions below 25 nm (Von Hofeten *et al* 2009).

6.3. XM-2 at the Advanced Light Source

The National Center for x-ray tomography at the Berkeley National Laboratory has recently completed the first soft x-ray microscope in the world designed specifically for cellular 3D imaging and complemented with cryogenic, high numerical aperture light microscopy, which is operated at the Advanced Light Source. Correlation of the cellular structure revealed by x-ray tomography with the location of fluorescence labeled biomolecules by the light microscopy is opening unprecedented opportunities to understand where in the cell the molecular interactions occur. Methods are being developed for high-throughput imaging of dynamic events in live cells using light microscopy and high-resolution analyses of those same cells using x-ray 3D imaging. Collection of tomography datasets is fully automated and can be accomplished in less than 3 min, revealing 3D images of structures throughout the entire cell. Figure 6.3 illustrates the tomographic reconstruction of C. albicans cells. The potential of the x-ray microscope to image fully hydrated cells has been demonstrated in reporting the detected sub-cellular changes resulting from the cellular response to peptoid treatment (Uchida *et al* 2009).

6.4. High-resolution x-ray imaging methods at the Advanced Photon Source

The Advanced Photon Source (APS) has made significant progress in the development of high-resolution x-ray imaging

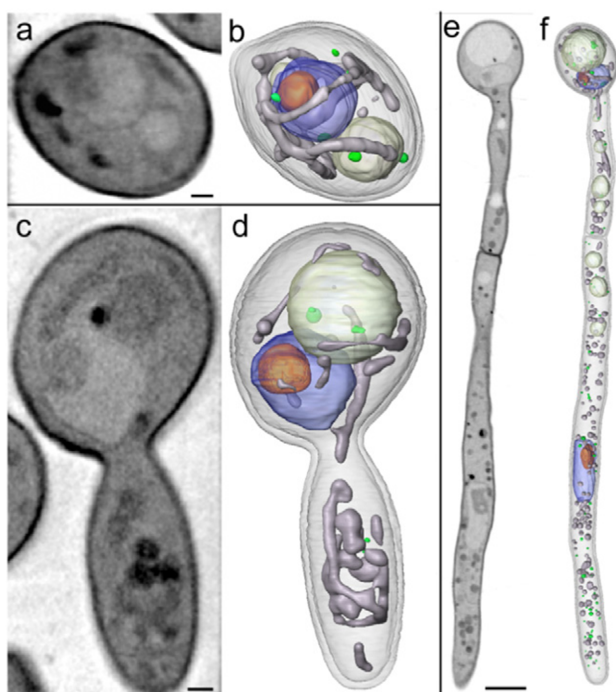

Figure 6.3. X-ray images (left) and corresponding tomographic reconstruction (right) of albicans cells for yeast-like ((a) and (b)), germ-like ((c) and (d)) and hyphal ((e) and (f)) cells. The volume rendered views (b), (d) and (f) show selected organelles that have been segmented: nucleus (blue), nucleolus (orange), mitochondria (gray), and lipid bodies (green) (Uchida *et al* 2009). Figure courtesy of Carolyn Larabell.

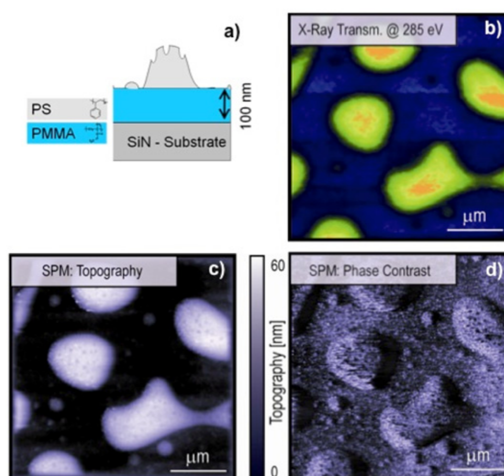

Figure 6.4. Imaging of the phase separation of a polymer blend (80% PMMA, 20% PS) with the recently installed NanoXAS instrument (Schmid *et al* 2010) of the Swiss Light Source. The specimen is illustrated in (a). The micrograph (b) shows the x-ray transmission micrograph in comparison to the topography (b) and phase contrast image (c) acquired with the scanning probe microscopy (SPM) mode of the instrument. Figure courtesy of Joerg Raabe. Q.C

methods and their application to materials, biological, and environmental science. Key areas where APS has established itself as a world leader are in three-dimensional (3D) and lensless coherent diffractive imaging. Both full-field and scanning instruments are in routine operation as user tools; x-ray phase and fluorescence contrast are the primary detection modes. A notable recent advance in 3D imaging includes quantitative mapping of trace metals and other elements in *Cyclotella meneghiniana* by scanning x-ray fluorescence tomography (De Jonge *et al* 2010). This highly sensitive approach to imaging showed that iron may serve as cofactor for some processes involved in silica deposition or metabolism via metalloproteins in this fresh-water diatom. Non-destructive analysis of the interior morphology and topology of dense material specimens at the nanoscale is practical via hard transmission microscopy, which was used to show that coarsening in nanoporous gold is governed by surface diffusion (Chen *et al* 2010). Coherent diffractive imaging, a method unbound by the limitations of x-ray optics technology, can be used to measure local strain as well as structure at nanometer resolution (Robinson *et al* 2010). Q.9 A resonant version of this method has been used to image the domain structure in magnetic multilayers with polarized x-rays. Use of multiple Bragg reflections enabled determination of the full nine-component strain tensor in a ZnO nanorod (Newton *et al* 2010).

6.5. NanoXAS at the Swiss Light Source

NanoXAS is a novel instrument at the Swiss Light Source that is aimed at combining the benefits of scanning force microscopy (AFM) with those of x-ray spectroscopy. The instrument combines a scanning transmission x-ray microscope with a beam-deflection atomic force microscope in a coaxial geometry, allowing *in situ* x-ray absorption spectroscopy and high-resolution topography measurements. When the conventional AFM scanning probe tip is replaced by a coaxially shielded tip the instrument allows detection of the photoelectrons produced by resonant x-ray absorption. This yields spectroscopic information with a spatial resolution approaching the values achievable with AFM (Schmid *et al* 2010).

The potential of the instrument is illustrated in figure 6.4, which shows the phase separation in a polymer blend (80% PMMA, 20% PS). A cut through the polymer blend is sketched in (a). The PMMA islands (yellow) embedded in the PS-matrix (blue) are clearly seen in the x-ray transmission image (b). Using the scanning probe microscopy (SPM) mode the height of the PMMA islands is ca. 45 nm according to the SPM topography (c). The SPM phase contrast (d) shows finer structures within the PS-matrix, although it is has worse quality due to a contaminated tip. Combining spectroscopic information from the x-rays with SPM data provides detailed information about the self-organization in such blends, in particular on defects, which are seen as dark spots on top of the PMMA islands (center) and differences between the bulk and surface structures.

6.6. The TwinMic microscope at Elettra

Having a closer look at the optical schemes of STXM and TXM instruments, both are similar, having the position of the lens

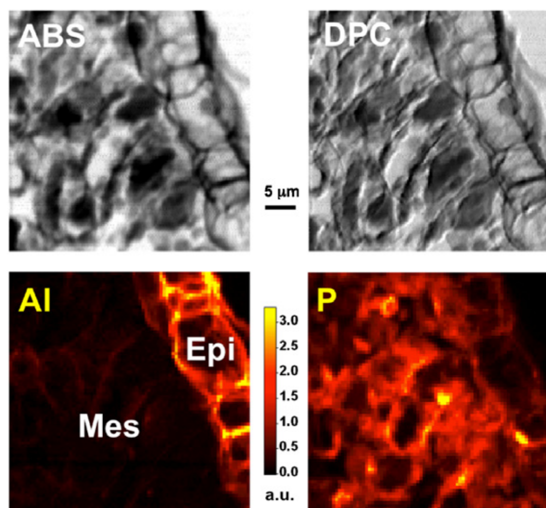

Figure 6.5. Tea plants hyperaccumulate Al, which is considered as a promoter for brain diseases such as Alzheimer's or Parkinson's. Top: absorption (ABS) and differential phase contrast images (DPC) of slices from tea leaves *Camellia sinensis*; bottom: Al and P LEXRF maps. LEXRF helps to understand the uptake, transport and tolerance of Al in tea plants. The concentration of Al in the membranes of mesophyll cells (Me) suggests that the retention of Al in epidermal leaf apoplast (Epi) represents the main tolerance mechanism of tea plants to Al. The low concentration of P in Al-rich regions indicates that P has no role in Al sequestration (Tolrà *et al* 2010). Figure courtesy of Katarina Vogel-Mikus and Roser Tolra.

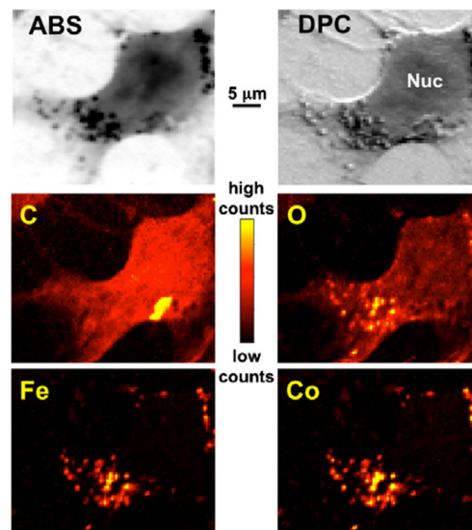

Figure 6.6. Uptake and interaction of $CoFe_2O_4$ engineered nanoparticles by mouse 3T3 fibroblast cells (Nuc is the nucleus). The absorption (ABS) and differential phase contrast (DPC) images show the morphology of the cell. LEXRF analysis of the C, O, Fe and Co. and semiquantitative analysis of the Fe and Co distribution within the cell reveal that Fe/Co stoichiometry changes when the nanoparticles enter the cell nucleus (Ceccone *et al* 2010). Figure courtesy of Giacomo Ceccone.

before and/or after the specimen and the role of the source and detector interchanged. This is defined as the reciprocity principle (Zeitler and Thomson 1970), which has been adapted to x-ray microscopy by Morrison *et al* (2002). In other words, for the TXM mode the condenser has to provide light with a high numerical aperture, whereas in STXM the detector has to collect the light with a wide angle.

Zeitler's reciprocity principle led to the idea of synergizing both imaging modes, STXM and TXM, into a *single* instrument. Starting from the year 2000, a consortium of European scientists started to investigate the feasibility of such a synergy, which led to the formation of the twin microscope 'TwinMic' (Kaulich *et al* 2006).

TwinMic is a soft x-ray transmission microscope working in the 400–2200 eV photon energy range with spatial resolution down to sub-50 nm, depending on the imaging mode and on the zone plate optics. The microscopy station is designed to address a broad variety of application fields, such as biology, biochemistry, biomineralization, pharmacology, nanotoxicology, environmental science, geochemistry, food science and new materials. It provides different contrast modes (absorption, darkfield, differential phase contrast, interference) that can be combined with chemical information retrieved from spectroscopy techniques like XANES, XRF and across-absorption-edge imaging (AAEI). The modular specimen environment can be operated in air, inert gas atmosphere or vacuum in order to adapt to different specimen characteristics.

In the STXM operation mode a FRCCD configurable detector provides absorption and differential phase contrast images (Morrison *et al* 2006), while silicon drift detectors (Alberti *et al* 2009) measure the LEXRF spectra of the specimen, thus allowing simultaneous collection of morphological and elemental information.

The high-resolution imaging and the chemical sensitivity of the TwinMic microscope have been recently employed to better understand the processes in biological systems occurring on sub-micron length scales. An example of TwinMic application in the food science field is depicted in figure 6.5. Aluminum is reported to be neurotoxic for many animal species and for men and it can be absorbed from the soil by plants, i.e. tea, through the roots. Figure 6.5 shows absorption and differential phase contrast images of a tea leaf (*Camellia sinensis*) section, collected in STXM mode, and the corresponding Al and P XRF maps, (Tolrà *et al* 2010), providing some insights about the uptake, the transport and the distribution of Al within the leaves.

Recent applications in the nanotoxicology field are focused on understanding the uptake mechanism and the effect of nanoparticles on cells status and some results are shown in figure 6.6. The absorption and the differential phase contrast images of a 3T3 mouse cell are shown together with the XRF elemental maps of Co and Fe (Ceccone *et al* 2010).

6.7. Magnetic imaging at the Advanced Light Source

Both STXM and TXM based techniques are capable of performing magnetic transmission x-ray microscopy using circularly polarized soft x-rays to achieve a strong magnetic contrast based on x-ray magnetic circular dichroism (XMCD) effects, which occur at selected absorption, e.g. L-edges of elements such as Fe, Co, Ni, etc. Combining high spatial resolution (better than 30 nm) and temporal resolution in the

sub-ns regime, limited by the inherent time structure of current synchrotron sources, x-ray magnetic microscopy can study the ultrafast dynamics of magnetic vortices and domain walls in confined ferromagnetic structures and stochastical behavior in the magnetization reversal process of thin films. The first magnetic imaging using STXM and TXM microscopes has been demonstrated by groups at ALS (Zhao *et al* 2006, Fischer and Im 2010). Very recent study reported direct observation of the stochastic behavior of the domain wall depinning field in notch-patterned Permalloy (Ni80Fe20) nanowires with different wire widths, thicknesses and notch depths with a lateral resolution of 15 nm by magnetic imaging with the TXM microscope at the ALS (Im *et al* 2009). Correlations between the magnetic behavior and the dimensions of the wires and notch depths are evidenced.

6.8. Nano-imaging and nano-analysis project NiNa at the European Synchrotron Facility

Driven by research areas with the highest scientific and societal impact, the upgrade of the ESRF beamline will be focused on biomedical studies, earth and environmental sciences, and nanotechnology. It will be a long, high brilliance beamline providing nano-focused beams for analytical imaging. The present conceptual design overcomes current ID22 limitations to meet the growing user demand and the requirement for improved spatial resolution. Based on a canted undulator solution, it calls for parallel operation of two nanoprobes. The NI end-station (Nano-Imaging) will mainly address problems in biology, biomedicine and nanotechnology using fluorescence analysis and nanotomography. It will be optimized for ultimate hard x-ray focusing of a beam with a large energy bandwidth at specific energies. Aiming at life science applications, it will operate in a cryo-environment. The NA end-station (Nano-Analysis) will offer a multi-analysis nanoprobe for spectroscopic studies (μ-XRF, μ-XAFS and μ-XRD) capable of *in situ* experiments at selective sub-micrometer scales. In a complementary way to the NI end-station, the NA end-station will provide a monochromatic beam tunable in a large energy range (Cloetens 2009).

6.9. The Nanoscopium project at Soleil

Nanoscopium is the single scanning hard x-ray nanoprobe beamline planned at SOLEIL. This ~155 m long beamline will fully exploit the high brilliance and coherence characteristics of the x-ray beam both for diffraction-limited focusing and for contrast formation. It will offer the most advanced imaging techniques in multimodal mode. The different scanning techniques offered by the operating instruments will permit elemental mapping at trace (ppm) levels (scanning XRF), speciation mapping (XANES), phase gradient mapping (differential phase contrast), and density contrast based imaging of internal structures (coherent diffraction imaging) down to 30 nm spatial resolution range. The beamline will share the SDL13 source straight section with the future tomography beamline by using canted undulators. The U20 in-vacuum undulator (minimum magnetic gap: 5.5 mm) of the Nanoscopium beamline will cover the 5–20 keV energy range without energy gaps. The stability of the nanobeam will be ensured by the horizontally reflecting beamline optics. A secondary source will be created by the sagittally and tangentially pre-focusing mirrors in front of the overfilled secondary slits. The trade off between high-energy resolution ($\Delta E/E \sim 10^4$) and high flux (10^{11} ph s^{-1} with $\Delta E/E \sim 10^2$) will be achieved by two interchangeable horizontally reflecting monochromators (a double crystal and a double multilayer one). A KB mirror and Fresnel zone plates will be used as focusing devices. The beamline is in the design and construction phase and is foreseen to be open for users in 2013 (Somogyi *et al* 2010).

6.10. The hard x-ray fluorescence microprobe beamline at the Australian source

A hard x-ray micro-nanoprobe has commenced operation at the Australian Synchrotron providing versatile x-ray fluorescence microscopy across an incident energy range from 4 to 25 keV. Two x-ray probes are used to collect μ-XRF and μ-XANES for elemental and chemical microanalysis: a Kirkpatrick–Baez mirror microprobe for micron resolution studies, and a Fresnel zone plate nanoprobe with laser interferometer position encoding capable of 60 nm resolution. The beamline is commissioning an advanced energy dispersive x-ray fluorescence detection scheme named Maia (Siddons *et al* 2004, Kirkham *et al* 2010). The Maia detector employs an annular geometry of a 384-element planar silicon array to create a large acceptance solid angle and handle count rates greater than 107 s^{-1}. On-the-fly scanning combined with event mode data acquisition enables sub-ms per virtual pixel dwell with real time elemental deconvolution and image projection. A 96-element Maia prototype has created high-definition elemental maps with over 100 megapixels on a range of geological, materials and biological samples in practical time frames. Ultrafast x-ray fluorescence acquisition enables high-definition elemental mapping, and creates the opportunity for fluorescence tomography and XANES imaging within practical time frames (Paterson *et al* 2007). Figure 6.7 gives an example of high-definition XRF mapping of a polished thin section of calcrete from the Mount Gibson gold deposit in Western Australia (Ryan *et al* 2009).

7. Concluding remarks and perspectives

From being rare and exotic instruments twenty years ago x-ray microscopes have become common and routinely used techniques and have opened unprecedented opportunities for characterization of a great variety of complex materials of various origins. X-ray microscopes are continuously enhancing their capabilities, adding new dimensions for expanding their applications, thanks to the growing number of synchrotron facilities and continuous improvements of the performance of synchrotron and laboratory x-ray sources, combined with noticeable recent progress in fabrication of x-ray optics reaching sub-10 nm spatial resolution, and advances in detection systems.

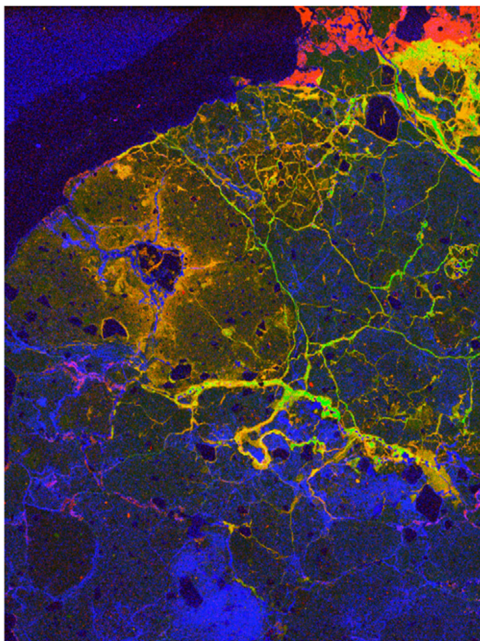

Figure 6.7. SXRF images of a geological sample using a 96-detector prototype of the Maia detector system (red = As, green = Fe, blue = Br). The detector is under development by CSIRO and BNL for installation on the XFM beamline at the Australian Synchrotron and X27A at the NSLS. The sample is a polished thin section of calcrete from the Mount Gibson gold deposit in Western Australia. The data were acquired at the XFM beamline using a beam spot size of ∼1.5 μm. The image area is 8.0 × 7.2 mm^2, 6400 pixels × 5760 pixels, each 1.25 μm (cropped from 12 × 10 mm^2, 9600 pixels × 8000 pixels), acquired using a transit time of 0.6 ms per pixel (Ryan *et al* 2009). Figure courtesy of Ryan and Paterson.

The rapidly growing demand for high-resolution tomography has led to the construction of modern cryo-transmission x-ray microscopes using laboratory or synchrotron x-ray sources, where collection and reconstruction of images is becoming faster and more routine and further improvements of lateral resolution for addressing phenomena down to a few nm length scales are expected in the near future.

Among the major developments of scanning x-ray microscopes is the continuous improvement of the transmission and energy resolution of x-ray and electron detectors in order to achieve nanometric spatial resolution in elemental and chemical mapping with extraordinary trace-element sensitivity.

Furthermoren, the optics-limited resolution of x-ray imaging in both full-field and scanning microscopes has been extended substantially by applying coherent diffraction and ptychography schemes, which can be implemented using x-ray sources with sufficiently high coherence and monitoring overlapping scan pixels with fast pixel-array detectors.

Indeed, it is not realistic using x-ray optics to push lateral resolutions below the nanometer range, but here steps in lensless coherent imaging where the resolution is diffraction-limited, i.e. dependent only on the wavelength of the x-ray source, have been made. However, coherent diffraction imaging does not give instant images and requires rather complicated resonant imaging schemes for retrieval of specific space-resolved information about the chemistry, electronic and magnetic properties of the specimen.

Q.14

Another increasingly demanded dimension is time resolution. Recently the most advanced full-field and scanning x-ray microscopes have allowed the following of a fast switching of magnetic vortices but still there are serious limits to exploring fast dynamic phenomena with chemical sensitivity and/or ultimate spatial resolution. Time-resolved x-ray microscopy, usually carried out using pump–probe schemes, is limited by the x-ray flux and pulse length of the synchrotron sources to tens of picosecond timescales. In this respect time-resolved coherent diffraction imaging studies are further limited by the partial coherence of the synchrotron sources to millisecond timescales.

One of the greatest opportunities for exploring dynamic phenomena by the combination of sub-nanoscale and atomic spatial resolution with temporal resolution down to femtosecond timescales of the atomic motion has been opened by coherent diffraction imaging using the coming to operation fully coherent and extremely bright x-ray free electron laser sources. Thanks to the ultimate peak brightness and ultra-short duration of x-ray pulses all speckle information can be collected in a single shot coherent imaging mode before the radiation damage manifests itself. The future ultrafast time-resolved coherent imaging at free electron laser facilities has the great potential to extend the insights obtained for static structures or structures undergoing slow temporal changes with synchrotron-based x-ray microscopy studies to ultrafast dynamic phenomena in complex functional natural or fabricated materials.

The multi-dimensional combination of nanoscale and atomic spatial resolution with chemical and temporal resolution constitutes one of the greatest opportunities for future studies of matter, which requires proper combination of x-ray microscopy and imaging approaches using both third and fourth generation sources, complemented with correlative studies with optical, electron, infrared and atomic probe microscopes.

Acknowledgments

We are grateful to our colleagues for sharing their results and for permission to publish their figures. In particular we wish to thank Giacomo Ceccone (European Joint Research Center, Ispra), Marine Cotte and Peter Cloetens (European Synchrotron Radiation Facility), Carolyn Larabell (National Center for X-ray Tomography at the Berkeley National Laboratory), Ian McNulty (Advanced Photon Source), David Paterson (Australian Synchrotron), Franz Pfeiffer (Technical University of Munich), Jörg Raabe (Swiss Light Source), Chris Ryan (CSIRO), Gerd Schneider (Helmholtz Center Berlin), Andrea Somogyi (Soleil), Tolek Tyliszczak (Advanced Light Source), Roser Tolra (Universitat Autonoma of Barcelona), and Ulrich Vogt (Biomedical and X-ray Physics Institute at the KTH Stockholm) for providing material and comments for this review.

We are indebted to past and current members of the Sincrotrone Trieste for their contributions to the development

of the TwinMic beamline and all their support in writing this review.

The European Commission under the Frame Programme 6 and contract number HRTI-2001-50024 funded the development of the TwinMic instrument.

PT acknowledges support through the DFG Cluster of Excellence 'Munich-Centre for Advanced Photonics'.

Q.15 **References**

Abbey B, Nugent K A, Williams G J, Clark J N, Peele A G, Pfeifer M A, de Jonge M and McNulty I 2008 *Nat. Phys.* 394–8 Q.16
Ade H and Hitchcock A P 2008 *Polymer* **49** 643–75
Ade H, Smith A P, Zhang H, Zhuang G R, Kirz J, Rightor E and Hitchcock A 1997 *J. Electron. Spectrosc. Relat. Phenom.* **84** 53–71
Alberti R, Klatka T, Longoni A, Bacescu D, Marcello A, De Marco A, Gianoncelli A and Kaulich B 2009 *X-ray Spectrom.* **38** 205–9
Allen L J, Faulkner H M L, Nugent K A, Oxley M P and Paganin D 2001 *Phys. Rev.* E **63** 376021
Als-Nielsen J and McMorrow D 2001 *Elements of Modern X-ray Physics* (New York: Wiley)
Anderson E H, Olynick D L, Harteneck B, Veklerov E, Denbeaux G, Chao W L, Lucero A, Johnson L and Attwood D 2000 *J. Vac. Sci. Technol.* B **18** 2970–5
Attwood D 1999 *Soft X-rays and Extreme Ultraviolet Radiation: Principles and Applications* (Cambridge: Cambridge University Press)
Attwood D 2004 *J. Phys. D: Appl. Phys.* **37** doi:10.1088/0022-3727/37/23/E01
Baez A V 1952 *J. Opt. Soc. Am.* **42** 405–12
Barrett R, Kaulich B, Salome M and Susini J 1999 Current status of the scanning x-ray microscope at the ESRF *X-ray Microscopy* vol 507, ed W Meyer-Ilse, A Warwick and D Attwood (New York: AIP) pp 458–63
Barty A 2008 *Phys. Rev. Lett.* **101** 055501
Barty A *et al* 2008 *Nat. Photon.* **2** 415–9
Bates R and Rodenburg J 1989 *Ultramicroscopy* **31** 303–7
Bates R H T 1982 *Optik* **61** 247–62
Bech M, Bunk O, David C, Ruth R, Rifkin J, Loewen R, Feidenhansl R and Pfeiffer F 2008 *J. Synchrotron Radiat.* **16** 43–7
Bergh M, Huldt G, Tímneanu N, Maia F R N C and Hajdu J 2008 *Q. Rev. Biophys.* **41** 181–204
Bertilson M C, Von Hofsten O, Lindblom M, Wilhein T, Hertz H M and Vogt U 2008 *Appl. Phys. Lett.* **92** 064104
Bleuet P, Gergaud P, Lemelle L, Tucoulou R, Cloetens P, Susini J, Delette G and Simionovici A 2010 *TrAC—Trends Anal. Chem.* **29** 518–27
Bogan M J *et al* 2008 *Nano Lett.* **8** 310–6
Bohic S, Simionovici A, Biquard X, Martinez-Criado G and Susini J 2005 *Oil Gas Sci. Technol.* **60** 979–93
Bonse U and Hart M 1965 *Appl. Phys. Lett.* **6** 155–6
Born M and Wolf E 1980 *Principles of Optics* (Oxford: Pergamon)
Brau C 1990 *Free-Electron Lasers* (Boston, MA: Academic)
Bruck Y M and Sodin L G 1979 *Opt. Commun.* **30** 304–8
Ceccone G, Marmorato P, Ponti J, Rossi F, Gianoncelli A, Pascolo L, Salomé M, Kaulich B and Kiskinova M 2010 *Nano Lett.* at press
Chao W, Anderson E H, Harteneck B D, Liddle J A and Attwood D T 2007 *AIP Conf. Proc.* **879** 1269–73
Chao W, Harteneck B D, Liddle J A, Anderson E H and Attwood D T 2005 *Nature* **435** 1210–3
Chao W, Kim J, Rekawa S, Fischer P and Anderson E H 2009 *Opt. Express* **17** 17669–77
Chao W, Tyliszczak T, Kim J, Fischer P, Rekawa S and Anderson E 2010 *AIP Conf. Proc.* in preparation Q.17
Chapman H N 1996 *Ultramicroscopy* **66** 153–72
Chapman H N 1997 *Scanning Microsc.* **11** 67–80
Chapman H N, Jacobsen C and Williams S 1995 *Rev. Sci. Instrum.* **66** 1332–4
Chapman H N, Jacobsen C and Williams S 1996 *Ultramicroscopy* **62** 191–213
Chapman H N *et al* 2006a *J. Opt. Soc. Am.* A **23** 1179–200
Chapman H N *et al* 2006b *Nat. Phys.* **2** 839–43
Charalambous P 2003 *J. Physique* IV **104** 185–8
Chen Y C, Chu Y, McNulty I, Shen Q, Voorhes P and Dunand D C 2010 *Appl. Phys. Lett.* **96** 043122
Cloetens P 2009 *Nano-imaging and Nanoanalysis; ESRF UPBL11 Conceptual Design Report* http://www.esrf.eu/UsersAndScience/Experiments/Imaging/beamline-portfolio/CDR_UPBL04_future-ID16.pdf
Cloetens P, Ludwig W, Baruchel J, Van Dyck D, Van Landuyt J, Guigay J P and Schlenker M 1999 *Appl. Phys. Lett.* **75** 2912–4
Cojoc D, Kaulich B, Carpentiero A, Cabrini S, Businaro L and Di Fabrizio E 2006 *Microelectron. Eng.* **83** 1360–3
Cosslet V E and Nixon W C 1951 *Nature* **168** 24–5
Cosslet V E and Nixon W C 1960 *X-ray Microscopy* (London: Cambridge University Press)
Cotte M and Susini J 2009 *MRS Bull.* **34** 403–5
Cotte M, Susini J, Dik J and Janssens K 2010 *Acc. Chem. Res.* **43** 705–14
David C, Nöhammer B, Solak H H and Ziegler E 2002 *Appl. Phys. Lett.* **81** 3287–9
David C, Thieme J, Guttmann P, Schneider G, Rudolph D and Schmahl G 1992 *Optik* **91** 95–9
David C *et al* 2003 *J. Physique* IV **104** 171–6
De Jonge M D, Hornberger B, Holzner C, Legnini D, Paterson D, McNulty I, Jacobsen C and Vogt S 2008 *Phys. Rev. Lett.* **100** 163902
De Jonge M D, Hornberger B, Holzner C, Twining B, Paterson D, McNulty I, Jacobsen C and Vogt S 2009 *J. Phys.: Conf. Ser.* **186** 012006
De Jonge M D *et al* 2010 *Proc. Natl Acad. Sci.* **107** 15676–80
Dierolf M, Menzel A, Thibault P, Schneider P, Kewish C M, Wepf R, Bunk O and Pfeiffer F 2010b *Nature* **467** 436–9
Dierolf M, Thibault P, Menzel A, Kewish C M, Jefimovs K, Schlichting I, König K, Bunk O and Pfeiffer F 2010a *New J. Phys.* **12** 035017
Di Fabrizio E, Cojoc D, Cabrini S, Kaulich B, Susini J, Facci P and Wilhein T 2003b *Opt. Express* **11** 2278–88
Di Fabrizio E, Kaulich B, Wilhein T and Susini J 2002 *Surf. Rev. Lett.* **9** 243–8
Di Fabrizio E, Romanato F, Gentili M, Cabrini S, Kaulich B, Susini J and Barrett R 1999 *Nature* **401** 895–8
Di Fabrizio E *et al* 2003a *Microelectron. Eng.* **67-8** 87–95
Einstein A 1918 *Verh. Dtsch. Phys. Ges.* **20** 86–7
Eisebitt S, Luning J, Schlotter W F, Lorgen M, Hellwig O, Eberhardt W and Stohr J 2004 *Nature* **432** 885–8
Elser V 2003a *J. Opt. Soc. Am.* A **20** 40–55
Elser V 2003b *Acta Crystallogr.* A **59** 201–9
Engstrom A 1946 *Acta Radiol.* **66** 1–106
Faulkner H M L and Rodenburg J M 2004 *Phys. Rev. Lett.* **93** 023903
Faulkner H M L and Rodenburg J M 2005 *Ultramicroscopy* **103** 153–64
Feser M, Duewer F, Wang S, Scott D, Lyon A and Yun W 2004 *Microsc. Microanal.* **10** 1036–7
Feser M, Hornberger B, Jacobsen C, De Geronimo G, Rehak P, Holl P and Strüder L 2006 *Nucl. Instrum. Methods Phys. Res.* A **565** 841–54
Fienup J R 1978 *Opt. Lett.* **3** 27–9
Fienup J R 1982 *Appl. Opt.* **21** 2758–69
Fischer P and Im M-Y 2010 *IEEE Photon. J.* **2** at press
Flank A M *et al* 2006 *Nucl. Instrum. Methods Phys. Res.* B **246** 269–74

Gabor D 1948 *Nature* **161** 777–8
Gelius U, Wannberg B, Baltzer P, Fellner-Feldegg H, Carlsson G, Johansson C G, Larsson J, Münger P and Vegerfors G 1990 *J. Electron Spectrosc. Relat. Phenom.* **52** 747–85
Gerchberg R W and Saxton W O 1972 *Optik* **35** 237–46
Gianoncelli A, Morrison G R, Kaulich B, Bacescu D and Kovac J 2006 *Appl. Phys. Lett.* **89** 251117
Giewekemeyer K, Thibault P, Kalbfleisch S, Beerlink A, Kewish C M, Dierolf M, Pfeiffer F and Salditt T 2010 *Proc. Natl Acad. Sci.* **107** 529
Guizar-Sicairos M and Fienup J R 2007 *Opt. Express* **15** 17592–612
Guizar-Sicairos M and Fienup J R 2008 *Opt. Express* **16** 7264–78
Gureyev T E 1999 *J. Phys. D: Appl. Phys.* **32** 563–7
Q.18 Hawkes P W 1978 *J. Opt. (Paris)* **9** 235–41
Hegerl R and Hoppe W 1970 *Ber. Bunsen-Ges. Phys. Chem.* **74** 1148–54
Heim S, Guttmann P, Rehbein S, Werner S and Schneider G 2009 *J. Phys.: Conf. Ser.* **186** 012041
Hertz H M *et al* 2003 *J. Physique* IV **104** 115–9
Hertz H M *et al* 2009 *J. Phys.: Conf. Ser.* **186** 012027
Hignette O, Cloetens P, Morawe C, Borel C, Ludwig W, Bernard P, Rommeveaux A and Bohic S 2007 *AIP Conf. Proc.* **879** 792–5
Hitchcock A P, Johansson G A, Mitchell G E, Keefe M H and Tyliszczak T 2008 *Appl. Phys.* A **92** 447–52
Holmberg A, Lindblom M, Reinspach J, Bertilsson M and Hertz H M 2009 *J. Phys.: Conf. Ser.* **186** 012065
Hornberger B, Feser M and Jacobsen C 2007 *Ultramicroscopy* **107** 644–55
Hornberger B *et al* 2008 *J. Synchrotron Radiat.* **15** 355–62
Horowitz P and Howell J A 1972 *Science* **178** 608–11
Howells H, Jacobsen C and Warwick A 2006 *Principles and Applications of Zone Plate X-ray Microscopes* (Berlin: Springer)
Howells M *et al* 2009 *J. Electron Spectrosc. Relat. Phenom.* **170** 4–12
Huang X *et al* 2009 *Phys. Rev. Lett.* **103** 198101
Ide-Ektessabi A 2007 *Applications of Synchrotron Radiation: Micro Beams in Cell Micro Biology and Medicine* (New York: Springer)
Im M Y, Bocklage L, Fischer P and Meier G 2009 *Phys. Rev. Lett.* **102** 147204
Jacobsen C, Beetz T, Feser M, Osanna A, Stein A and Wirick S 2002 *Surf. Rev. Lett.* **9** 185–91
Jacobsen C, Feser M, Lerotic M, Vogt S, Maser J and Schäfer T 2003 *J. Physique* IV **104** 623–6
Jacobsen C, Wirick S, Flynn G and Zimba C 2000 *J. Microsc. —Oxford* **197** 173–84
Janssens K *et al* 2000 *X-ray Spectrom.* **29** 73–91
Jenkins R 1999 *X-ray Fluorescence Spectrometry* (New York: Wiley)
Jensen T H, Bech M, Bunk O, Donath T, David C, Feidenhans' L R and Pfeiffer F 2010 *Phys. Med. Biol.* **55** 3317–23
Jochum L and Meyer-Ilse W 1995 *Appl. Opt.* **34** 4944–50
Joyeux D, Polack F and Phallipou D 1999 *Rev. Sci. Instrum.* **70** 2921–6
Kagoshima Y, Yokoyama K, Nimi T, Koyama T, Tsusaka Y, Matsui J and Takai K 2003 *J. Physique* IV **104** 49–52
Kang H C *et al* 2008 *Appl. Phys. Lett.* **92** 221114
Kaulich B, Oestreich S, Salome M, Barrett R, Susini J, Wilhein T, Di Fabrizio E, Gentili M and Charalambous P 1999 *Appl. Phys. Lett.* **75** 4061–3
Kaulich B, Polack F, Neuhaeusler U, Susini J, di Fabrizio E and Wilhein T 2002a *Opt. Express* **10** 1111–7
Kaulich B, Wilhein T, Di Fabrizio E, Romanato F, Altissimo M, Cabrini S, Fayard B and Susini J 2002b *J. Opt. Soc. Am.* **19** 797–806
Kaulich B *et al* 2006 *Conf. Proc. IPAP* **7** 22–5
Kenney J M *et al* 1984 *Nucl. Instrum. Methods Phys. Res.* A **222** 37–41
Kern D *et al* 1984 Electron beam fabrication and characterization of Fresnel zone plates for soft x-ray microscopy *Science with Soft X-rays* vol 447, ed F J Himpsel and R W Klaffky (Bellingham, WC: SPIE) pp 204–13
Kewish C M, Thibault P, Dierolf M, Bunk O, Menzel A, Vila-Comamala J, Jefimovs K and Pfeiffer F 2010a *Ultramicroscopy* **110** 325–9
Kewish C M, Thibault P, Bunk O and Pfeiffer F 2010b *New J. Phys.* **12** 035005
Kilcoyne A L D *et al* 2003 *J. Synchrotron Radiat.* **10** 125–36
Kirkham R *et al* 2010 *AIP Conf. Ser.* **1234** 240–3
Kirkpatrick P and Baez A V 1948 *J. Opt. Soc. Am.* **38** 766–74
Kirz J and Jacobsen C 2009 *J. Phys.: Conf. Ser.* **186** 012001
Kirz J, Jacobsen C and Howells M 1995 *Q. Rev. Biophys.* **28** 33–130
Kirz J and Sayre D (ed) 1980 Soft x-ray microscopy of biological specimens *Synchrotron Radiation Research* (New York: Plenum)
Kiskinova M 2003 *J. Physique* **104** 453–8
Kohmura Y, Takano H, Suzuki Y and Ishikawa T 2003 *J. Physique* IV **104** 571–4
Krause M O 1979 *J. Phys. Chem. Rev. Data* **8** 307–27
Kumakhov M A 1990 *Nucl. Instrum. Methods Phys. Res.* B **48** 283–6
Kumakhov M A 2000 *Proc. SPIE—The Int. Soc. Opt. Eng.* **4155** 2–12
Lahlil S, Biron I, Cotte M and Susini J 2010a *Appl. Phys.* A 1–10
Lahlil S, Biron I, Cotte M, Susini J and Menguy N 2010b *Appl. Phys.* A **98** 1–8
Le Gros M A, McDermott G and Larabell C A 2005 *Curr. Opin. Struct. Biol.* **15** 593–600
Lengeler B, Schroer C, Tummler J, Benner B, Richwin M, Snigirev A, Snigireva I and Drakopoulos M 1999 *J. Synchrotron Radiat.* **6** 1153–67
Lerotic M, Jacobsen C, Schafer T and Vogt S 2004 *Ultramicroscopy* **100** 35–57
Lima E, Wiegart L, Pernot P, Howells M, Timmins J, Zontone F and Madsen A 2009 *Phys. Rev. Lett.* **103** 198102
Maiden A M and Rodenburg J M 2009 *Ultramicroscopy* **109** 1256–62
Marchesini S, He H, Chapman H N, Hau-Riege S P, Noy A, Howells M R, Weierstall U and Spence J C H 2003 *Phys. Rev.* B **68** 1401011
Marchesini S *et al* 2008 *Nat. Photon.* **2** 560–3
Maser J *et al* 2006 *IPAP Conf. Ser.* **7** 26–9
Mayo S C, Davis T J, Gureyev T E, Miller P R, Paganin D, Pogany A, Stevenson A W and Wilkins S W 2003b *Opt. Express* **11** 2289–302
Mayo S C *et al* 2002 *J. Microsc.* **207** 79–96
Mayo S C *et al* 2003a *J. Physique* IV **104** 543–6
McNulty I, Kirz J, Jacobsen C, Anderson E H, Howells M R and Kern D P 1992 *Science* **256** 1009–12
McNulty I *et al* 2003 *J. Physique* IV **104** 11–15
Medenwaldt R and Uggerhoj E 1998 *Rev. Sci. Instrum.* **69** 2974–7
Menzel A, Kewish C M, Dierolf M, Thibault P, Kraft P, Bunk O, Jefimovs K, David C and Pfeiffer F 2009 *J. Phys.: Conf. Ser.* **186** 012054
Meyer-Ilse W *et al* 1995 *Synchrotron Radiat. News* **8** 29–33
Miao J, Charalambous P, Kirz J and Sayre D 1999 *Nature* **400** 342–4
Miao J, Hodgson K O, Ishikawa T, Larabell C A, A L G M and Nishino Y 2003 *Proc. Natl Acad. Sci. USA* **100** 110–2 Q.19
Miao J, Ishikawa T, Johnson B, Anderson E H, Lai B and Hodgson K O 2002 *Phys. Rev. Lett.* **89** 088303
Michette A G 1986 *Optical Systems for Soft X-rays* (New York: Plenum)
Mimura H *et al* 2010 *Nat. Phys.* **6** 122–5
Mollenstedt G, von Grote K H and Jonsson C 1963 Production of Fresnel zone plates for extreme ultraviolet and soft x radiation *X-ray Optics and X-ray Microanalysis* ed H H Pattee, V E Cosslet and A Engstrom (New York: Academic) pp 73–9
Momose A, Takeda T and Itai Y 1995 *Rev. Sci. Instrum.* **66** 1434–6

Morrison G, Gianoncelli A, Kaulich B, Bacescu D and Kovac J 2006 *Conf. Proc. Ser. IPAP* **7** 377–9
Morrison G R 1993 San Diego, CA, USA, Publ by Int Soc for Optical Engineering
Q.20
Morrison G R and Browne M T 1992 *Rev. Sci. Instrum.* **63** 611–4
Morrison G R, Eaton W J and Charalambous P 2002 *J. Physique* IV **104** 547–50
Morrison G R, Hare A R and Burge R E 1987 *Proc. Institute of Physics Electron Microscopy and Analysis Group Conference* (Bristol: Institute of Physics) pp 333–6
Morrison G R and Niemann B 1996 Differential phase contrast x-ray microscopy *X-ray Microscopy and Spectromicroscopy* ed J Thieme, D Rudolph, G Schmahl and E Umbach (Berlin: Springer) pp I-85–94
Murty M V R K 1963 *J. Opt. Soc. Am.* **53** 568–70
Myers O E 1951 *Am. J. Phys.* **19** 359–65
Nellist P, McCallum B C and Rodenburg J M 1995 *Nature* **374** 630–2
Nelson J, Huang X, Steinbrener J, Shapiro D, Kirz J, Marchesini S, Neiman A M, Turner J J and Jacobsen C 2010 *Proc. Natl Acad. Sci. USA* **107** 7235
Neuhausler U, Schneider G, Ludwig W, Meyer M A, Zschech E and Hambach D 2003 *J. Phys. D: Appl. Phys.* **36** A79–82
Neutze R, Wouts R, van der Spoel D, Weckert E and Hajdu J 2000 *Nature* **406** 752–7
Newberry S P and Summers S E 1956 *Int. Conf. on Electron Microscopy* vol 1954 (London: Royal Microscopical Society) pp 305–7
Newton M C, Leake S J, Harder R and Robinson I K 2010 *Nat. Mater.* **9** 120
Niemann B, Guttmann P, Hambach D, Schneider G, Weiss D and Schmahl G 2001 *Nucl. Instrum. Methods Phys. Res.* A **467** 857–60
Niemann B, Rudolph D and Schmahl G 1974 *Opt. Commun.* **12** 160–3
Niemann B, Rudolph D and Schmahl G 1976 *Appl. Opt.* **15** 1883–4
Nishino Y, Takahashi Y, Imamoto N, Ishikawa T and Maeshima K 2009 *Phys. Rev. Lett.* **102** 18101
Nishiwaki Y, Nakanishi T, Terada Y, Ninomiya T and Nakai I 2006 *X-ray Spectrom.* **35** 195–9
Nixon W C 1955 *Proc. R. Soc.* A **232** 475–85
Nugent K A 2009 *Adv. Phys.* **59** 1–99
Nugent K A, Peele A G, Quiney H M and Chapman H N 2005 *Acta Crystallogr.* A **61** 373–81
Ojeda-Castaneda J and Gomez-Reino C C 1996 Selected papers on zone plates *SPIE Press Book* (Bellingham, WA: SPIE Optical Engineering Press)
Ortega R, Devès G and Carmona A 2009a *J. R. Soc. Interface* **6** 649–58
Ortega R *et al* 2009b *Toxicol. Lett.* **188** 26–32
Paganin D, Mayo S C, Gureyev T E, Miller P R and Wilkins S W 2002 *J. Microsc.* **206** 33–40
Pagot E, Cloetens P, Fiedler S, Bravin A, Coan P, Baruchel J, Härtwig J and Thomlinson W 2003 *Appl. Phys. Lett.* **82** 3421–3
Palmer J R and Morrison G 1991 *OSA Proc. on Short Wavelength Coherent Radiation: Generation and Applications* vol 11 (Washington, DC: Optical Society of America) pp 141–5
Paterson D J, Boldeman J W, Cohen D D and Ryan C G 2007 *AIP Conf. Proc.* **879** 864–7
Pereiro E, Nicolas J, Ferrer S and Howells M R 2009 *J. Synchrotron Radiat.* **16** 505–12
Pfeifer M A, Williams G J, Vartanyants I A, Harder R and Robinson I K 2006 *Nature* **442** 63–6
Pfeiffer F, Bech M, Bunk O, Donath T, Henrich B, Kraft P and David C 2009 *J. Appl. Phys.* **105** 102006
Pfeiffer F, Bech M, Bunk O, Kraft P, Eikenberry E F, Brönnimann C, Grünzweig C and David C 2008 *Nat. Mater.* **7** 134–7
Pfeiffer F, Kottler C, Bunk O and David C 2007 *Phys. Rev. Lett.* **98** 108105
Podorov S G, Pavlov K M and Paganin D M 2007 *Opt. Express* **15** 9954–62
Pogani A *et al* 1997 *Rev. Sci. Instrum.* **68** 2774–82
Polack F, Joyeux D, Svalos D and Phallipou D 1995 *Rev. Sci. Instrum.* **66** 2180
Raabe J, Watts B, Tzetkov G, Fink R H and Quitmann C 2008 *J. Phys.: Conf. Ser.* **186** 102102
Rarback H *et al* 1990a *J. X-ray Sci. Technol.* **2** 274–96
Rarback H *et al* 1990b *Nucl. Instrum. Methods Phys. Res.* A **291** 54–9
Rau C, Somogyi A, Bytchkov A and Simionovici A 2001 *SPIE* **4503** 14–22
Ravasio A *et al* 2009 *Phys. Rev. Lett.* **103** 028104
Rayleigh L 1888 *Encyclopedia Brittanica XXIV*
Q.21
Rehbein S, Holmberg A, Johansson G A, Jansson P A C and Hertz H M 2004 *J. Vac. Sci. Technol.* B **22** 1118–22
Reichelt R 2006 *Scanning Electron Microscopy* (Berlin: Springer)
Robinson I and Harder R 2009 *Nat. Mater.* **8** 291–8
Rodenburg J M 2008 Ptychography and related diffractive imaging methods *Adv. Imaging Electron. Phys.* **150** 87–184
Rodenburg J M and Bates R H T 1992 *Phil. Trans. R. Soc.* A **339** 521–53
Rodenburg J M and Faulkner H M L 2004 *Appl. Phys. Lett.* **85** 4795–7
Rodenburg J M, Hurst A C and Cullis A G 2007a *Ultramicroscopy* **107** 227–31
Rodenburg J M, Hurst A C, Dobson B R, Pfeiffer F, Bunk O, David C, Jefimovs K and Johnson I 2007b *Phys. Rev. Lett.* **98** 1–4
Rodrigues M S, Dhez O, Denmat S, Chevrier J, Felici R and Comin F 2008 *J. Instrum.* **3** P12004–11
Roentgen W C 1896 *Nature* **53** 274–6
Rose H 1974 *Optik* **39** 416–36
Rose V, Freeland J W, Gray K E and Streiffer S K 2008 *Appl. Phys. Lett.* **92** 193510
Rudolph D, Niemann B, Schmahl G and Christ O 1984 *X-ray Microscopy, Goettingen* (*Springer Series in Optical Sciences*) (Berlin: Springer)
Russel Luke D 2005 *Inverse Problems* **21** 37–50
Ryan C G *et al* 2009 *AIP Conf. Proc.* **1221** 9–17
Sakdinawat A and Liu Y 2007 *Opt. Lett.* **32** 2635–7
Sakdinawat A and Liu Y 2008 *SPIE* **6883** 68803V
Salomé M *et al* 2009 *J. Phys.: Conf. Ser.* **186** 012014
Sandberg R, Raymondson D, La-O-Vorakiat C, Paul A, Raines K, Miao J, Murnane M, Kapteyn H and Schlotter W 2009 *Opt. Lett.* **34** 1618–20
Sandberg R L *et al* 2008 *Proc. Natl Acad. Sci. USA* **105** 24
Sarrazin P, Blake D, Feldman S, Chipera S, Vaniman D and Bish D 2005 *Powder Diffract.* **20** 128–33
Sayre D 1952 *Acta Crystallogr.* **5** 843–5
Sayre D 1972 *Tech. Rep.* IBM T. J. Watson Research LaboratoryYorktown Heights RC 3974 New York p RC 3974
Sayre D 1980 Prospects for long-wavelength x-ray microscopy and diffraction *Imaging Processes and Coherence in Physics* vol 112 (Berlin: Springer) pp 229–35
Sayre D 2008 *Acta Crystallogr.* A **64** 33–5
Schlotter W F *et al* 2007 *Opt. Lett.* **32** 3110–2
Schmahl G and Rudolph D 1969 *Optik* **29** 577
Schmahl G and Rudolph D 1987 Proposal for a phase contrast x-ray microscope *X-ray Microscopy: Instrumentation and Biological Applications* ed P C Cheng and G J Jan (Berlin: Springer) pp 231–8
Schmahl G, Rudolph D, Guttmann P, Schneider G, Thieme J and Niemann B 1995 *Rev. Sci. Instrum.* **66** 1282–6
Schmahl G, Rudolph D, Schneider G, Guttmann P and Niemann B 1994 *Optik* **97** 181–2
Schmid I, Raabe J, Sarafimov B, Quitmann C, Vranjkovic S, Pellmont Y and Hug H J 2010 *Ultramicroscopy* at press
Schneider G 1998 *Ultramicroscopy* **75** 85–104
Schroer C G *et al* 2008 *Phys. Rev. Lett.* **101** 090801

Schroer C G *et al* 2010 *Nucl. Instrum. Methods Phys. Res.* A **616** 93–7
Schropp A *et al* 2010 *Appl. Phys. Lett.* **96** 091102
Schwarzschild B 2008 *Phys. Today* **61** 12–6
Scott D, Duewer F, Kamath S, Lyon A, Trapp D, Wang S and Yun W 2004 *Worcester, MA*
Shannon C E 1949 *Proc. IRE* **37** 10–21
Shapiro D *et al* 2005 *Proc. Natl Acad. Sci. USA* **102** 15343–6
Shen Q, Bazarov I and Thibault P 2004 J. *Synchrotron Radiat.* **11** 432–8
Siddons D P, Beuttenmuller R H, O'Connor P, Kuczewski A J and Li Z 2004 *AIP Conf. Proc.* **705** 953–6
Siegbahn K 1990 *J. Electron. Spectrosc. Relat. Phenom.* **51** 11–36
Somogyi A, Polack F and Moreno T 2010 *AIP Conf. Proc.* **1234** 395–8
Soret J L 1875 *Annal. Physik. Chem.* **156** 99–113
Spector S, Jacobsen C and Tennant D M 1997 *J. Vac. Sci. Technol.* A **15** 2872–6
Stampanoni M, Groso A, Pfeiffer F, Bunk O, Weitkamp T, Diaz A and David C 2006 *3rd IEEE Int. Symp. Biomedical Imaging* pp 1100–3
Stohr J 1992 *NEXAFS Spectroscopy* (Berlin: Springer)
Stroke G W 1965 *Appl. Phys. Lett.* **6** 201–3
Stuik R, Shmaenok L A, Fledderus H, Andreev S S, Shamov E A, Zuev S Y, Salashchenko N N and Bijkerk F 1999 *J. Anal. At. Spectrom.* **14** 387–90
Susini J, Barrett R, Kaulich B, Oestreich S and Salome M 1999 The x-ray microscopy facility at the ESRF: a status report *X-ray Microscopy* vol 507, ed W Meyer-Ilse, A Warwick and D Attwood (New York: AIP) pp 19–27
Susini J, Salomé M, Fayard B, Eichert D, Dhez O and Tucoulou R 2004 *Microsc. Microanal.* **10** 124–5
Susini J, Salome M, Fayard B, Ortega R and Kaulich B 2002 *Surf. Rev. Lett.* **9** 203–11
Susini J *et al* 2006 *IPAP Conf. Ser.* **7** 18–21
Sutton M, Mochrie S, Greytak T, Nagler S and Berman L 1991 *Nature* **352** 608–10
Suzuki Y, Awaji M, Takeuchi A, Takano H, Uesugi K, Kohmura Y, Kamijo N, Yasumoto M and Tamura S 2003 *J. Physique* IV **104** 35–40
Suzuki Y and Uchida F 1995 *Rev. Sci. Instrum.* **66** 1468–70
Takemoto K *et al* 2003 *J. Physique* IV **104** 57–61
Takman P A C, Stollberg H, Johansson G A, Holmberg A, Lindblom M and Hertz H M 2007 *J. Microsc.* **226** 175–81
Teague M R 1983 *J. Opt. Soc. Am.* A **73** 1434–41
Tennant D M, Raab E L, Becker M M, O'Malley M L, Bjoerkholm J E and Epworth R W 1990 *J. Vac. Sci. Technol.* B **8** 1970–4
Thibault P, Dierolf M, Kewish C M, Menzel A, Bunk O and Pfeiffer F 2009a *Phys. Rev.* A **80** 043813
Thibault P, Dierolf M, Menzel A, Bunk O, David C and Pfeiffer F 2008 *Science* **321** 379–82
Thibault P, Dierolf M, Menzel A, Bunk O and Pfeiffer F 2009b *Ultramicroscopy* **109** 338–43
Tieg C *et al* 2010 *J. Phys.: Conf. Ser.* **211** 012024
Tolrà R *et al* 2010 *J. Plant Res.* doi:10.1007/s10265-010-0344-3 **Q.22**
Tsusaka Y, Yokoyama K, Takeda S, Takai K, Kagoshima Y and Matsui J 2001 *Nucl. Instrum. Methods Phys. Res.* A **467/468** 670–3
Tyliszczak T, Kilcoyne A L D, Liddle J A, Warwick T, Hitchcock A P, Ade H and Shuh D K 2004 *Microsc. Microanal.* **10** 1018–9
Uchida M, McDermott G, Wetzler M, Le Gros M A, Myllys M, Knoechel C, Barron A E and Larabell C A 2009 *Proc. Natl Acad. Sci. USA* **106** 19375–80
Urquhart S G and Ade H 2002 *J. Phys. Chem.* B **106** 8531–8
Vila-Comamala J *et al* 2009 *J. Phys.: Conf. Ser.* **186** 012078
Vogt S, Chapman H N, Jacobsen C and Medenwaldt R 2001 *Ultramicroscopy* **87** 25–44
Vogt U, Lindblom M, Charalambous P, Kaulich B and Wilhein T 2006 *Opt. Lett.* **31** 1465–7
Vogt U, Lindblom M, Jansson P A C, Tuohimaa T T, Holmberg A, Hertz H M, Wieland M and Wilhein T 2005 *Opt. Lett.* **30** 2167–9
Von Hofeten O, Bertilson M, Reinspach J, Holmberg A, Hertz H M and Vogt U 2009 *Opt. Lett.* **34** 2631–3
Walther A 1963 *Acta Opt.* **10** 41–9
Weiss D, Peuker M and Schneider G 1998 *Appl. Phys. Lett.* **72** 1805–7
Weitkamp T, Rau C, Snigirev A, Drakopoulos M and Simionovici A 2000 *IEEE Nuclear Science Symp. Conf. Record* vol 3, p 19/1
Werner S, Rehbein S, Guttmann P, Heim S and Schneider G 2009 *J. Phys.: Conf. Ser.* **186** 012079
Wilhein T, Kaulich B, Di Fabrizio E, Romanato F, Cabrini S and Susini J 2001 *Appl. Phys. Lett.* **78** 2082–4
Williams G J, Pfeifer M A, Vartanyants I A and Robinson I K 2003 *Phys. Rev. Lett.* **90** 175501
Williams G J, Quiney H M, Dhal B B, Tran C Q, Nugent K A, Peele A G, Patterson D and de Jonge M D 2006 *Phys. Rev. Lett.* **97** 1–4
Wolf E 1962 *Proc. Phys. Soc.* **80** 1269–72
Yada K and Takahashi S 1992 *X-ray Microscopy III* (London: Springer)
Youn H S, Baik S Y and Chang C H 2005 *Rev. Sci. Instrum.* **76** 023702
Yun W-B, Kirz J and Sayre D 1987 *Acta Crystallogr.* A **43** 131–3
Zeitler E and Thomson M G R 1970 *Optik (Stuttgart)* **31** 258–80
Zernike F 1935 *Physik. Z.* **36** 848–51
Zhang X, Ade H, Jacobsen C, Kirz J, Lindaas S, Williams S and Wirick S 1994 *Nucl. Instrum. Methods Phys. Res.* A **347** 431–5
Zhao T *et al* 2006 *Nat. Mater.* **5** 823–9
Zhu D *et al* 2010 *Phys. Rev. Lett.* **105** 043901

Queries for IOP paper 220805

Journal: **JPhysCM**
Author: **B Kaulich et al**
Short title: **Transmission and emission x-ray microscopy**

Page 1

Query 1:
Author: Please check the author names and affiliations carefully.

Query 2:
Author: Please be aware that the colour figures in this article will only appear in colour in the Web version. If you require colour in the printed journal and have not previously arranged it, please contact the Production Editor now.

Page 3

Query 3:-
Author: Kenney *et al* (1983) changed to Kenney *et al* (1984). Please check.

Page 4

Query 4:-
Author: Pogany *et al* (1997) changed to Pogani *et al* (1997) as per reference list. Please check.

Page 7

Query 5:
Author: Please check 'speciation' here.

Page 8

Query 6:
Author: Please check 'such as' here.

Query 7:-
Author: Rodenburg *et al* (2007) changed to Rodenburg *et al* (2007a) and Rodenburg *et al* (2007b) here. Please check.

Page 9

Query A:
Author: Figures 4.3 and 5.3 not cited in text. Please check.

Page 11

Query 8:
Author: Please check 'speciation' here.

Page 14

Query B:
Author: Please check 'imposed' here.

Page 16

Query 9:-
Author: 'Robinson *et al* 2010' not in the reference list. Please check.

Query C:
Author: (b) seems to stand for two different things in figure 6.4. Please check.

Page 18

Query 10:
Author: Please check whether '80' and '20' be subscripts here.

Query 11:
Author: Please check 'wire widths' here.

Query 12:
Author: Please check 'NiNa' given in the heading of subsection 6.8 but 'NI' and 'NA' given in the paragraph below.'

Query 13:
Author: 'Soleil' given in the heading of subsection 6.9 but 'SOLEIL' given in the paragraph below. Please check.

Page 19

Query 14:
Author: Please check 'have been made' here.

Page 20

Query 15:-
Author: Please check the details for any journal references that do not have a blue link as they may contain some incorrect information. Pale purple links are used for references to arXiv e-prints.

Query 16:-
Author: Abbey *et al* (2008), Lahlil *et al* (2010a): Please provide volume.

Query 17:-
Author: Chao *et al* (2010), Fischer and Im (2010), Schmid *et al* (2010): Any update.

Page 21

Query 18:-
Author: Hawkes (1978): Please check the journal title.

Query 19:-
Author: Miao *et al* (2003): Please check the fifth author name.

Page 22

Query 20:-
Author: Morrison (1993), Scott *et al* (2004): Any more details?

Query 21:-
Author: Rayleigh (1888): Please provide publisher and place.

Page 23

Query 22:-

Author: Tolrà *et al* (2010): Please provide volume and page/article number.